Bioactive Materials 46 (2025) 118–133

Contents lists available at ScienceDirect

Bioactive Materials

journal homepage: www.keaipublishing.com/en/journals/bioactive-materials

Copper–luteolin nanocomplexes for Mediating multifaceted regulation of oxidative stress, intestinal barrier, and gut microbiota in inflammatory bowel disease

Wanyue Fu [a,1], Zhongshi Huang [b,1], Weiqi Li [a,1], Lingling Xu [a], Miaomiao Yang [c], Yan Ma [a], Hanghang Liu [b,***], Haisheng Qian [a,**], Wanni Wang [a,*]

[a] School of Biomedical Engineering, Anhui Provincial Institute of Translational Medicine, Anhui Engineering Research Center for Medical Micro-Nano Devices, Anhui Medical University, Hefei, 230011, PR China
[b] Hubei Key Laboratory of Natural Products Research and Development, College of Biological and Pharmaceutical Sciences, China Three Gorges University, Yichang, 443002, PR China
[c] The First Affiliated Hospital of Anhui Medical University, Anhui Public Health Clinical Center, Hefei, 230012, PR China

ARTICLE INFO

Keywords:
Inflammatory bowel disease
Regulating inflammatory microenvironment
Oxidative stress
Reactive oxygen species
Flora regulation
Nrf2/NF-κB

ABSTRACT

Oxidative stress, dysbiosis, and immune dysregulation have been confirmed to play pivotal roles in the complex pathogenesis of inflammatory bowel disease (IBD). Herein, we design copper ion–luteolin nanocomplexes (CuL NCs) through a metal–polyphenol coordination strategy, which plays a multifaceted role in the amelioration of IBD. The fabricated CuL NCs function as therapeutic agents with exceptional antioxidant and anti-inflammatory capabilities because of their great stability and capacity to scavenge reactive oxygen species (ROS). It can effectively modulate the inflammatory microenvironment including facilitating the efficient reduction of pro-inflammatory cytokine levels, protecting intestinal epithelial cells, promoting mucosal barrier repair and regulating intestinal microbiota. In addition, CuL NCs have been found to enhance cellular antioxidant and anti-inflammatory capacities by regulating the nuclear factor erythroid 2–related factor 2/heme oxygenase-1 (Nrf2/HO-1) oxidative stress pathway and nuclear factor kappa B (NF-κB) signaling pathway, respectively. Notably, CuL NCs demonstrate significant prophylactic and therapeutic efficacy in mouse models with typical IBD, including ulcerative colitis (UC) and Crohn's disease (CD). This study provides a new approach for building multifaceted therapeutic platforms for natural products to treat IBD.

1. Introduction

Inflammatory bowel disease (IBD) is a chronic inflammatory disorder with a rapidly increasing incidence worldwide, particularly in newly industrialized countries [1,2]. The pathogenesis of IBD is associated with oxidative stress, inflammatory response, disruption of intestinal barrier function, imbalance of the gut microbiota, and dysregulation of the mucosal immune system [3]. Traditional treatment for IBD usually includes medications, nutritional interventions, and surgical procedures. Commonly used medications include 5-aminosalicylic acid (5-ASA) [4], corticosteroids, immunosuppressants (such as azathioprine and methotrexate), and biologics (such as antitumor necrosis factor-α antibodies) [5]. Although these treatments can relieve symptoms and control inflammation, they often fail to fundamentally solve IBD, and long-term use may lead to side effects and drug resistance [6]. Furthermore, the longer the duration of inflammation, the higher the risk of intestinal and systemic complications. Therefore, developing a rapid and effective strategy is key to treating IBD.

During the development of IBD, complex molecular interactions and cellular communications occur between different proinflammatory cytokines, chemokines, inflammatory cells, and immune cells [7]. (1) Oxidative Stress and Cellular Damage: excess reactive oxygen species

* Corresponding author.
** Corresponding author.
*** Corresponding author.
E-mail addresses: liuhanghang@ctgu.edu.cn (H. Liu), shqian@ahmu.edu.cn (H. Qian), wnwang@ahmu.edu.cn (W. Wang).
[1] These authors contributed equally to this work.

https://doi.org/10.1016/j.bioactmat.2024.12.004
Received 14 September 2024; Received in revised form 2 December 2024; Accepted 2 December 2024

(ROS) present in the inflammatory microenvironment are higher than normal levels [8]. Intestinal epithelial cell damage is caused by the imbalance in oxidative stress due to a large concentration of ROS and a diminished antioxidant capacity. This imbalance leads to oxidation of proteins and lipids and damage of DNA molecules. (2) Intestinal Barrier Disruption and Inflammation: the intestinal mechanical barrier is damaged by the loss of intestinal epithelial cells, and colonic tissue damage is worsened by the entry of neutrophils and other pathogens [9,10]. Alternatively, excessive ROS affect macrophage differentiation and activate inflammatory factors, causing inflammation [11]. M2 macrophages, which play a role in immunosuppression and tissue repair, typically produce minimal anti-inflammatory cytokines. This leads to chronic inflammation, and a sequence of inflammatory cascade reactions are triggered [12]. (3) Microbial Imbalance: growing evidence shows that intestinal inflammation and permeability issues caused by microbial imbalance play important roles in the progression of IBD [13]. Restoring intestinal homeostasis is a complex challenge that cannot be addressed through a single therapeutic approach. Therefore, there is an urgent need to develop a range of multidimensional regulatory strategies that not only alleviate the symptoms of the inflammatory microenvironment in the gut but also facilitate better long-term management outcomes, thereby ensuring safe and effective treatment of IBD [14,15].

Natural active small molecules (NASMs) demonstrate promise for treating IBD, offering benefits such as minimal side effects, affordability, and easy accessibility [16–18]. For example, epigallocatechin gallate (EGCG) primarily found in green tea exhibits anti-inflammatory, antioxidant, and antibacterial effects [19]. Tea polyphenols can inhibit intestinal inflammation and improve the gut microbiota [20]. Luteolin (Lut) is a flavonoid with unique antioxidant properties and has garnered considerable attention owing to its diverse biological activities, including anti-inflammatory, anticancer, and cardiovascular protective effects [21,22]. Lut has demonstrated remarkable efficacy in modulating the nuclear factor erythroid 2–related factor 2 (Nrf2) signaling pathway [23,24]. It exerts its effects by upregulating antioxidant enzyme genes such as heme oxygenase-1 (HO-1) and NAD(P)H quinone oxidoreductase 1 (NQO1), thereby mitigating oxidative stress, and by targeting proinflammatory cytokines such as tumor necrosis factor-α (TNF-α) and interleukin-6 (IL-6) to suppress inflammation [25–27]. Consequently, the modulation of Nrf2 by Lut is considered an effective strategy for management of colitis. However, the application of NASMs is frequently constrained by challenges such as instability, insufficient targeting, and low bioavailability[28,29]. Additionally, Lut is susceptible to oxidative degradation because of its highly unsaturated structure, which restricts its solubility and bioavailability in water [30].

Herein, we develop copper ion–Lut nanocomplexes (CuL NCs) using a metal–polyphenol coordination strategy through a simple hybrid approach. This strategy of nanometrization of NASMs using metal ions can effectively address their low bioavailability [31–33]. Copper (Cu) is an essential trace element for the human body. Cu exists in its oxidized (Cu^{2+}) and reduced (Cu^{+}) forms, and both forms have inherent redox properties that are vital for maintaining redox homeostasis [34,35]. Therefore, it can be hypothesized that the complexation of the copper ion with Lut may enhance the enzymatic catalytic performance and antioxidant activity of Lut, thereby improving overall ROS scavenging efficiency and bioavailability of Lut. As illustrated in Scheme 1, the highly stable CuL NCs can effectively reduce the excess ROS in the inflammatory lesions in the intestine, and protecting intestinal epithelial cells. While promoting the polarization of macrophages toward the M2 phenotype, CuL NCs also facilitate the nuclear translocation of Nrf2, which activates the expression of downstream antioxidant enzymes HO-1 to combat oxidative stress damage. Furthermore, CuL NCs inhibit the nuclear factor kappa B (NF-κB) signaling pathway by downregulating phosphorylated IκB kinase β (p-IκKβ) and phosphorylated NF-κB p65 (p-p65), thereby reducing proinflammatory factors and effectively modulating the imbalance of oxidative stress and excessive inflammation. Additionally, CuL NCs restore the levels of tight junction–related proteins, improving intestinal barrier function while enhancing the abundance and diversity of the gut microbiota. This study aims to clarify that metal–polyphenol coordination with multifaceted regulation of the inflammatory microenvironment could be a novel approach for management of IBD.

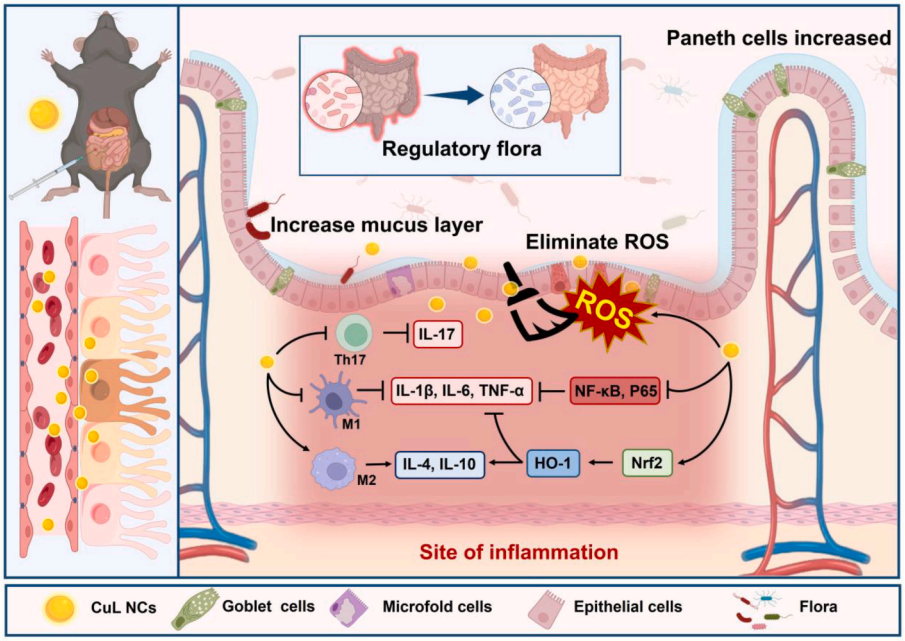

Scheme 1. Schematic of CuL NCs in the treatment of IBD. CuL NCs reduces intestinal oxidative stress and inflammation through Nrf2 activation and NF-κB inhibition, protects intestinal epithelial cells while inhibiting further intestinal damage, improves intestinal barrier function, and enhances the abundance and diversity of intestinal flora.

2. Materials and methods

2.1. Synthesis of CuL NCs

First, polyvinyl pyrrolidone (PVP; 1200 mg) was dissolved in 40 mL of deionized water. Then, 210 mg of anhydrous copper (II) sulfate ($CuSO_4$) powder was added to the solution and stirred until clear. Lut (40 mg) was added, and the solution was stirred at 25°C for 72 h and then centrifuged at 10,000 rpm for 10 min to remove excess Lut. The supernatant containing CuL NCs was filtered using a 100-KD ultrafiltration tube to eliminate excess PVP and Cu ions. Finally, the resulting CuL NCs were stored at 4 °C for future use.

2.2. Cell viability assay

RAW264.7, HT-29 [36–38], NCM460 [39], L929, and HUVEC cells were cultured until they reached the logarithmic growth phase. They were then digested and plated into 96-well plates at a density of 1×10^4 cells per well. After overnight incubation for cell adherence, the old medium was discarded. Next, the medium with varying concentrations of CuL NCs was added, and the solution was incubated for 24 h. 3-(4, 5-Dimethylthiazol-2-yl)-2,5-diphenyltetrazolium bromide (MTT) was added, and the solution was incubated for 4 h. Dimethyl sulfoxide (DMSO) was added, and absorbance was read at 490 nm. The cell survival rate was calculated based on the absorbance results. OD_1: indicates the OD value of the experimental group; OD_2: indicates the OD value of the blank group; OD_3: indicates the OD value of the control group.

$$\text{Cell Viability}\ (\%) = \frac{OD_1 - OD_2}{OD_3 - OD_2} \times 100\%$$

2.3. Cell uptake

RAW264.7 cells were inoculated in confocal dishes with approximately 1×10^6 cells per well and cultured for 1 day to ensure cell attachment. The groups are as follows: control group = no Cy5.5-CuL NCs are added; low-concentration group = 100 μg/mL of Cy5.5-CuL NCs are added; high-concentration group = 200 μg/mL Cy5.5-CuL NCs are added. Culture of cells was continued for 6 h to allow endocytosis of CuL NCs. After treatment, the culture was gently rinsed with phosphate buffered saline (PBS) to eliminate any CuL NCs that were not endocytosed. The cells were fixed with 4 % paraformaldehyde for 15–30 min and then washed with PBS.

2.4. Nrf2 immunofluorescence

RAW264.7 cells were inoculated at 1×10^6 cells per well in confocal dishes and incubated for 12 h. The supernatant was absorbed, lipopolysaccharide (LPS) (1 μg/mL) was added with Dulbecco's modification of Eagle's medium (DMEM), 1 mL of the configured solution was added, and the solution was incubated for 12 h. Bovine serum albumin (BSA) was sealed for 2 h and added to cell permeable solution, and the Nrf2 antibody was applied and incubated at 37 °C for 4 h. The cells were rinsed with PBS, and then the secondary antibody was incubated for 30 min. After the addition of 4′,6-diamidino-2-phenylindole (DAPI), images of the sealed sheet were taken using a fluorescence microscope.

2.5. Anti-inflammatory experiment

RAW264.7 cells were plated in 24-well plates. After incubating for 24 h, cells were induced by 1 μg/mL LPS and different concentrations of CuL NCs for additional 12 h of incubation. The supernatant was analyzed via the enzyme-linked immunosorbent assay (ELISA) kit. The mRNA expression of antioxidant antioxidative genes was also measured through quantitative Realreal-time polymerase chain reaction PCR (qRT-PCR) assay (Table S1).

2.6. In vivo imaging system (IVIS)

Healthy mice were intraperitoneally injected with 20 mg/kg of Cy5.5-CuL NCs and imaged at 0, 2, 4, 8, 12, 24, and 48 h after injection via IVIS imaging. Major organs of sacrificed mice (heart, liver, spleen, lungs, kidneys, and colon) were taken for IVIS imaging at 0, 2, 4, 8, 12, 24, and 48 h.

2.7. DSS-induced colitis model

Preventive experimental groups were established as follows: (1) PBS + water, (2) CuL NCs (5, 10, and 20 mg/kg) + water, (3) PBS + 4 % DSS, and (4) 4 % DSS + CuL NCs (5, 10, and 20 mg/kg). After one week of adaptation, (1) and (2) were given drinking water for 7 days, while (3) and (4) were given 4%w/v DSS water for 7 days. Fresh DSS drinking water was prepared and old ones were replaced every 2 days. (1) and (3) were intraperitoneally injected with PBS on days 1, 3, and 5, while (2) and (4) were intraperitoneally injected with CuL NCs on days 1, 3, and 5. Daily assessment includes recording weights and calculating the disease activity index (DAI) scores (Table S2). All mice were euthanized, and the entire colon and other internal organs were extracted. The colon length of each group was then measured and photographed (n = 4).

Preventive experimental groups were established as follows: (1) PBS + water, (2) PBS + 4 % DSS, (3) 4 % DSS + PVP, (4) 4 % DSS + Cu^{2+}, (5) 4 % DSS + Lut, (6) 4 % DSS + Lut + Cu^{2+}, (7) 4 % DSS + Mesalazine (5-ASA), (8) 4 % DSS + CuL NCs (20 mg/kg). After one week of adaptation, (1) was given normal drinking water for 7 days, while (2) ~ (8) were given 4%w/v DSS water for 7 days. Fresh DSS drinking water was prepared and old ones were replaced every 2 days. (1) and (2) were intraperitoneally injected with PBS on days 1, 3, and 5, while (3) ~ (8) were intraperitoneally injected with PVP, Cu^{2+}, Lut, Lut + Cu^{2+}, 5-ASA and CuL NCs, respectively, on days 1, 3, and 5. The concentrations of both Cu^{2+} and Lut were at the same level as that of CuL NCs (n = 5).

Colitis treatment groups were established as follows: (1) PBS + water, (2) PBS + 4 % DSS, (3) 4 % DSS + CuL NCs (10 mg/kg), and (4) 4 % DSS + CuL NCs (20 mg/kg). After one week of adaptation, (1) was given drinking water for 7 days, while (2) ~ (4) were given 4%w/v DSS water for 7 days. Fresh DSS drinking water was prepared and old ones were replaced every 2 days. (1) and (2) were intraperitoneally injected with PBS on day 8, 10, 12, and 14, while (3) and (4) were intraperitoneally injected with CuL NCs on days 8, 10, 12, and 14. Body weight, mouse status (Table S3), and DAI score were recorded. On day 16, the mice were killed and the whole colon and organs were taken. The colons of each group were recorded (n = 5).

2.8. TNBS-induced Crohn's disease (CD) model

Crohn's disease (CD) mice treatment groups were established as follows: (1) control group, (2) 2,4,6-trinitrobenzene sulfonic acid (TNBS) group, (3) TNBS + 10 mg/kg CuL NCs group, and (4) TNBS + 20 mg/kg CuL NCs group. There were eight mice in each group. All the mice acclimated for a week, and then before the TNBS-induced colitis model was constructed, the mice were fasted overnight. The (1), (2), and (3) group were given 2 % TNBS/ethanol enema. Subsequently, mice in the (3) and (4) groups were intraperitoneally injected with 10 and 20 mg/kg of CuL NCs from the first day to the fifth day, respectively. Simultaneously, the control and TNBS groups received intraperitoneal injections of PBS solution. Observations were made regarding body weight, fecal consistency, the presence of blood in the stool, DAI scores, and the overall physical condition and activity levels of the mice.

2.9. Histological evaluation

Samples were preserved in 4 % paraformaldehyde solution to maintain tissue structure. The fixed tissue samples were dehydrated and then treated with xylene to remove water. The sample was then

immersed in paraffin until fully embedded. The paraffin-embedded tissue was cut into sections that were 5–10 μm thick using a microtome and placed on a slide. For frozen slices, PBS washing was performed. For paraffin sections, dewaxing and hydration were performed. Hematoxylin and eosin (H&E) or Alcian Blue–periodic acid–Schiff staining (AB-PAS) was performed. After the sheet was sealed, the slices were observed to record the tissue structure, cell morphology, and other characteristics. The stained tissues were scored according to Table S4.

2.10. Immunohistochemistry (IHC) and immunofluorescence (IF)

IHC staining: Sections are dewaxed in xylene and passed through a series of ethanol solutions (100 %, 95 %, and 70 %). The sections were boiled in sodium citrate solution for antigen repair. The slices were incubated with blocking solution and incubated at 4 °C overnight for the primary antibody. The secondary antibodies were incubated for 30–60 min. 3,3′-Diaminobenzidine (DBA) solution was added, and hematoxylin was mixed for staining. Finally, the sections were observed under an optical microscope. IF staining: Fresh colon tissue of mice was frozen and incubated using a tyramide signal amplification (TSA) kit. Then, the tissue was observed under a fluorescence microscope.

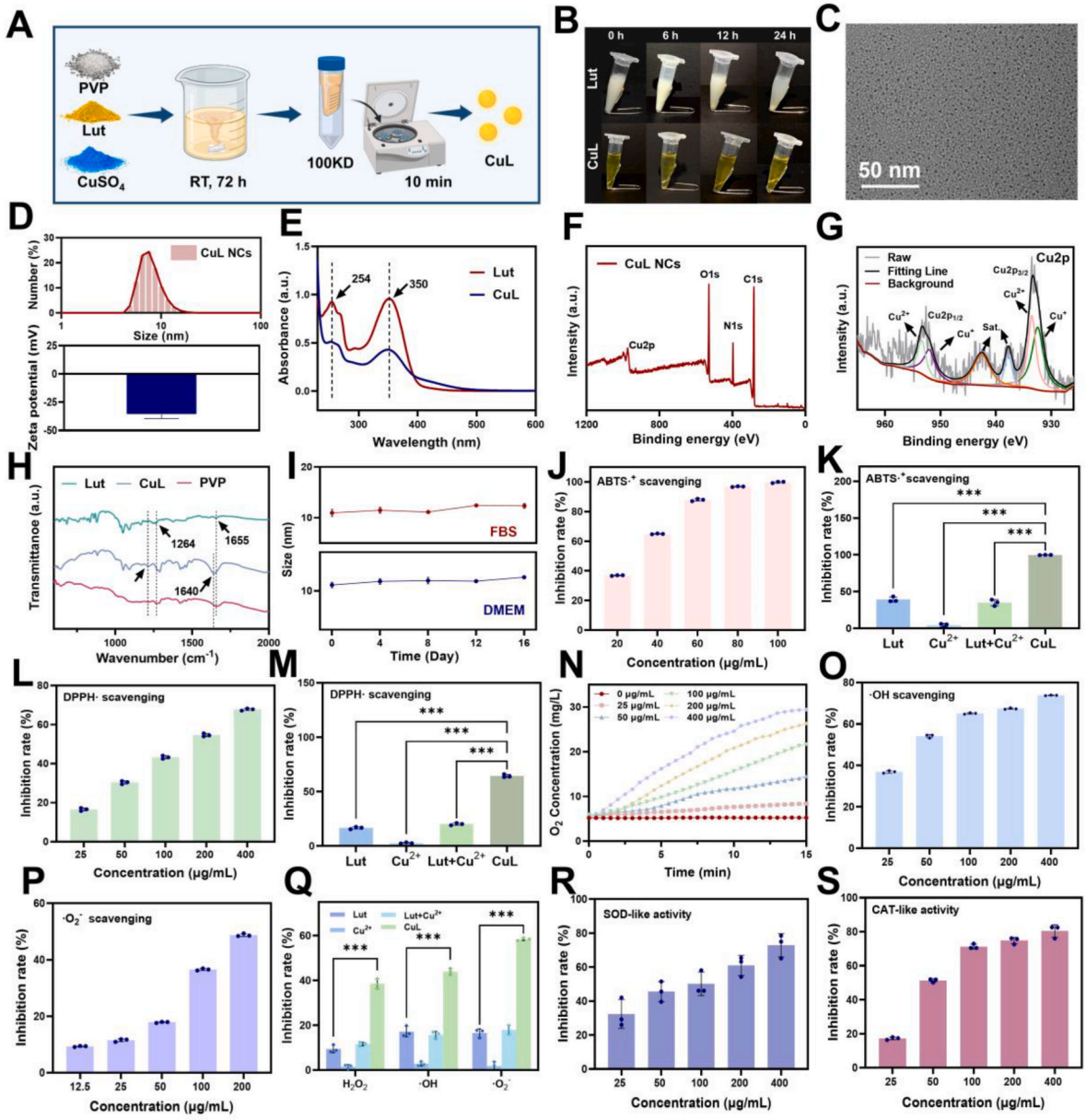

Fig. 1. Synthesis and characterization of CuL NCs. (A) Synthesis of CuL NCs. (B) Comparison of Lut and CuL NCs (at the same amount of Lut). (C) TEM images; scale bar = 50 nm. (D) Size distribution by DLS and Zeta potential. (E) UV–vis spectra of Lut and CuL NCs. (F, G) XPS patterns of CuL NCs and Cu2p. (H) FT-IR spectra of Lut, CuL NCs and PVP. (I) Hydrodynamic size of CuL NCs in different solutions. (J) Different concentrations of CuL NCs ABTS·$^{+}$ scavenging activity. (K) ABTS·$^{+}$ scavenging activity (the concentrations of both copper ions and Lut at the same level as that of CuL NCs. CuL NCs = 100 μg/mL). (L) Different concentrations of CuL NCs DPPH· scavenging activity. (M) DPPH· scavenging activity (the concentrations of both copper ions and Lut at the same level as that of CuL NCs. CuL NCs = 100 μg/mL). (N–P) H_2O_2, ·OH, and $\cdot O_2^-$ scavenging activities. (Q) H_2O_2, H_2O_2, and $\cdot O_2^-$ scavenging activity was observed when the concentrations of copper ions and Lut were maintained at the same level in the CuL NCs (CuL NCs = 100 μg/mL). (R, S) SOD-like and CAT-like antioxidative activity of CuL NCs. The data are presented as the mean ± standard deviation (SD) with (n = 3).

2.11. Statistical analysis

Data are presented as mean ± standard deviation (SD). The experimental data and differences were analyzed using GraphPad Prism 9.5 software (GraphPad, San Diego, CA) through one-way analysis of variance (ANOVA) followed by Tukey's multiple comparisons test. Significant differences among groups were indicated as $^{*}P < 0.05$, $^{**}P < 0.01$, and $^{***}P < 0.001$. A P-value of less than 0.05 was considered statistically significant, corresponding to a 95 % confidence level.

2.12. Animals

Male C57BL/6 mice and male BALB/c nude mice (6 weeks old) were obtained from Henan Skobes Biotechnology Co., Ltd. All the animal studies were approved by the Association of Laboratory Animal Sciences and the Center for Laboratory Animal Sciences at Anhui Medical University.

2.13. Ethics approval statement

All animal experiments received approval from the Ethics Committee of Anhui Medical University (approval number: LLSC20241722). These experiments were conducted in compliance with the guidelines set forth by the Association of Laboratory Animal Sciences and the Center for Laboratory Animal Sciences at Anhui Medical University.

3. Results and discussion

3.1. Synthesis and characterization of CuL NCs

Herein, anhydrous $CuSO_4$ was mixed with Lut solution in the presence of PVP at room temperature to obtain CuL NCs (Fig. 1A). In Fig. 1B, Lut exhibits relatively low water solubility, leading to noticeable precipitation after 12 h. However, upon complexation with copper ions, the solution changes to a clear and transparent yellow color, demonstrating a stable form. Transmission electron microscopy (TEM) images show that the CuL NCs have a uniform particle size distribution (Fig. 1C), with an average size of 7.58 ± 0.90 nm (Fig. 1D). Additionally, the Zeta potential is measured at −35.7 ± 3.83 mV. Compared with Lut solution, the characteristic absorption peaks of Lut appear at 254 and 350 nm, and similar characteristic peaks of CuL NCs also appear at these two places, indicating the successful complexation of Lut [40] (Fig. 1E). The X-ray diffraction (XRD) pattern in Fig. S1 indicates that CuL NCs are amorphous, with no crystalline copper-containing phase detected. In Fig. 1F, the X-ray photoelectron spectroscopy (XPS) spectrum displays peaks associated with the Cu, O, N, and C elements at binding energies of 974, 529, 397, and 282 eV, respectively. After deconvolution, the Cu 2p spectrum of CuL NCs reveals six peaks (Fig. 1G). The high-resolution Cu 2p spectrum shows a main peak for Cu $2p_{3/2}$ at 933.3 eV and a main peak for Cu $2p_{1/2}$ at 953.3 eV. The peak at 933.3 eV is deconvoluted into two peaks that correspond to Cu^{2+} (933.5 eV) and Cu^{+} (932.5 eV), confirming the presence of two oxidation states in CuL NCs. Moreover, the composition and structure of CuL NCs were characterized by Fourier transform infrared spectroscopy (FT-IR) (Fig. 1H). The absorption peak at 1264 cm^{-1}, which is attributed to the stretching vibration of the C–O bond of the phenolic hydroxyl group coupled with the in-plane bending vibration of the O–H bond in Lut, shows a shift after the formation of the nanocomplexes. The tensile vibration peak of the carbonyl group (C=O) shifts from 1655 to 1640 cm^{-1}, which further demonstrates the successful complexation of copper ions with Lut [41]. Thermogravimetric analysis (TGA) was used to estimate Lut content in CuL NCs (Fig. S2) [42]. The weight loss of CuL NCs occurred in three distinct stages. The first stage, observed around 100 °C, was attributed to the evaporation of water. The second stage occurred at 240–349 °C was associated with the thermal decomposition of a mixed species of Lut and PVP [43,44]. The third stage of weight loss, occurring between 450 and 800 °C, was associated with the thermal decomposition of the remaining Lut [45]. In summary, the weight percentage of Lut in the CuL NCs is approximately 14.25 wt%. While inductively coupled plasma mass spectrometry (ICP-OES) analysis determined that Cu ions constituted 4.14 wt %. Additionally, dynamic light scattering (DLS) (Fig. 1I) and ζ potential (Fig. S3) measurements demonstrate that CuL NCs maintain remarkable stability in various physiological solutions, such as fetal bovine serum (FBS) and DMEM. These results demonstrate the successful synthesis of CuL NCs nanocomplexes through the coordination of Cu ions with Lut and their good stability.

3.2. ROS scavenging activity of CuL NCs

Considering that the broad-spectrum antioxidant activity of newly developed nanomedicines is one of the key factors in the treatment of IBD, the antioxidant activity of CuL NCs need to be investigated. Redox potential measures the ability of a compound to gain or lose electrons. The reduction potential of CuL NCs was found to be lower than that of Lut, suggesting that CuL NCs had stronger antioxidant capacity than Lut (Fig. S4) [46–48]. Various Cu valence states in CuL NCs, along with the inherent antioxidant properties of Lut, indicate potential SOD-like and CAT-like catalytic mechanisms. As illustrated in Fig. S5, Cu^{+} is oxidized by $\cdot O_2^-$ to Cu^{2+}, producing H_2O_2, while the hydroxyl group of Lut donates electrons to $\cdot O_2^-$, forming additional H_2O_2. Cu^{2+} can be reduced back to Cu^{+} by oxidizing $\cdot O_2^-$ to O_2. The valence transition of Cu in CuL NCs is crucial for the $\cdot O_2^-$ disproportionation reaction. The unique CAT-mimicking activity of CuL NCs likely stems from the Cu^{+} coordination structure, which catalyzes the decomposition of H_2O_2 into O_2 and H_2O_2 [49]. $ABTS^{\cdot+}$, a typical ROS-related derivative, was completely eliminated by 100 μg/mL of CuL NCs (Fig. 1J and S6). For a comparison, the $ABTS^{\cdot+}$ scavenging abilities of Lut, Cu ions, mixtures of Lut and Cu ions and CuL NCs were examined. It was demonstrated that CuL NCs exhibited strong $ABTS^{\cdot+}$ scavenging ability (Fig. 1K). CuL NCs at a concentration of 400 μg/mL eliminated about 70 % of nitrogen radicals with numerous unpaired electrons (Fig. 1L and S7). CuL NCs also exhibited greater antioxidant activity than Lut, Cu ions, and mixtures of Lut and Cu ions (Fig. 1M).

We conducted further investigations into the ROS scavenging capability of CuL NCs by assessing their effectiveness against three representative ROS: H_2O_2, $\cdot O_2^-$, and ·OH. First, the levels of oxygen produced by different concentrations of CuL NCs after a 15-min reaction were recorded using a dissolved oxygen meter. Fig. 1N shows that the concentration of dissolved oxygen in CuL NCs levels off when it reaches a certain level, eventually producing ~30 mg/L of O_2 when the CuL NCs concentration is 400 μg/mL ·OH, which is a highly toxic and destructive ROS, exhibited a stronger scavenging effect with increasing CuL NCs concentration (Fig. 1O and Fig. S8). Subsequently, the scavenging ability of CuL NCs for $\cdot O_2^-$ was investigated separately using a superoxide anion detection kit, and the scavenging ability of CuL NCs for $\cdot O_2^-$ was found to steadily improve at each concentration gradient (Fig. 1P). Analysis of the results indicates that CuL NCs exhibit a stronger capacity to scavenge H_2O_2, ·OH, and $\cdot O_2^-$ than Lut, Cu ions, and a mixture of Lut and Cu ions at the same concentration (Fig. 1Q). In addition, CuL NCs have been shown to exhibit SOD-like and CAT-like activities using the total SOD activity assay kit and the CAT activity assay kit, respectively. The concentration of CuL NCs was positively correlated with SOD- and CAT-like activities, and 400 μg/mL of CuL NCs exhibited SOD-like and CAT-like activities of 72 ± 6.9 % and 80 ± 3.7 %, respectively, showing satisfactory activity effects (Fig. 1R and S).

3.3. Cytoprotective capacity and anti-inflammatory effects of CuL NCs In vitro

After demonstrating the excellent ROS scavenging ability of CuL NCs, RAW264.7 and HT-29 cells were chosen to evaluate the effect of different concentrations of CuL NCs on cell viability. After incubating

the cells with different concentrations of CuL NCs for up to 24 h, CuL NCs exhibited good biocompatibility and low toxicity, with the relative viability of the cells maintained at >80 % even at CuL NCs concentration as high as 200 μg/mL (Fig. 2A and **B**). Additionally, CuL NCs showed similar results for NCM460, L929, and HUVEC cells (Fig. S9). These experimental results demonstrate that CuL NCs do not cause significant toxicity to the cells, prompting us to continue to investigate their cellular uptake behavior. The cell uptake characteristics of Cy5.5-CuL NCs were evaluated after coincubation with RAW264.7 cells. In the control group, only blue fluorescence was produced by DAPI staining and no red fluorescence could be observed. In the experimental group, in addition to blue fluorescence, red fluorescence of CuL NCs was observed around the nucleus and the red fluorescence intensity showed a marked increase with increasing concentration of CuL NCs (Fig. 2C).

Using the endocytosis property combined with the ROS scavenging effect of CuL NCs, the antioxidant properties of CuL NCs were further evaluated at the cellular level. RAW264.7 cells were stimulated with H_2O_2 to generate intracellular ROS and were then treated with CuL NCs [50,51]. A notable enhancement in cell viability was observed in RAW264.7 cells treated with CuL NCs compared to those subjected to H_2O_2-induced damage without treatment with CuL NCs (Fig. 2D). Similarly, CuL NCs enhanced the viability of HT-29 cells after H_2O_2-induced oxidative stress injury (Fig. 2E). Furthermore, CuL NCs exhibited enhanced cytoprotective effects compared to Cu ions, Lut, and the mixture of Lut and copper ions (Fig. S10). To observe the protective effect of CuL NCs on cells more directly, live/dead cell staining was performed on RAW264.7 cells. Almost no cell death was observed in the cells incubated with CuL NCs alone, while the RAW264.7 cells subjected to continuous stimulation with H_2O_2 on a large area died, showing a large amount of red fluorescence (Fig. 2F). However, in the experimental group pretreated with different concentrations of CuL NCs, the fluorescence images showed that cell viability recovered to varying degrees, and after treatment with 200 μg/mL of CuL NCs, cells almost returned to their normal state. Notably, CuL NCs also played a protective role in HT-29 cells against oxidative stress (Fig. S11). Compared with the same-concentration a mixture of Lut and Cu ions treatment group, the CuL NCs treatment group showed better resistance to H_2O_2-induced cell death (Fig. S12).

Afterward, the ability of CuL NCs to scavenge intracellular ROS was assessed. During cell growth in a logarithmic period, high concentration of H_2O_2 was used as an exogenous stimulus to incubate RAW264.7 cells to induce oxidative stress, at which time a large amount of ROS was generated inside the cells. As demonstrated in Fig. 2G, the control group without H_2O_2 exhibited no significant green fluorescence. This suggests that the levels of ROS generated were insufficient to impact the observations when the cells were undergoing normal physiological metabolism. By contrast, there was a large amount of green fluorescence in the experimental group that added only H_2O_2, indicating that exogenous H_2O_2 successfully induced oxidative stress in the cells. In the 100-μg/mL CuL NCs group, the green fluorescence was reduced in some cells, while at a dose of 200 μg/mL, it was almost invisible, clearly suggesting that CuL NCs eliminated the intracellular ROS. Similar results were confirmed in HT-29 cells (Fig. S13). In comparison with Lut and Cu ions separately, excess ROS and free radical production led to oxidative stress in RAW264.7 cells, resulting in constitutive damage to the nuclear junctions. By contrast, a natural oval shape was observed in the nuclei of all the cells treated with CuL NCs (Fig. S14). Effects of CuL NCs on the ROS levels of RAW264.7 and HT-29 cells were further quantified across a broad concentration range using flow cytometry. After exogenous H_2O_2 stimulation, the relative fluorescence intensity of cells increased. Notably, the relative fluorescence intensity decreased more significantly at higher concentrations of CuL NCs, indicating that CuL NCs have a concentration-dependent ability to scavenge ROS (Fig. S15). In addition, excess ROS production led to a decrease in mitochondrial membrane potential (MMP), which triggered the release of proapoptotic factors such as cytochrome *c* from the mitochondria. This process activates downstream apoptotic signaling pathways, ultimately causing cell death [52]. To evaluate the impact of CuL NCs on MMP, cells were exposed to H_2O_2, which resulted in a decrease in red fluorescence and an increase in green fluorescence, indicating that the generation of free radicals caused mitochondrial damage, causing a reduction in MMP. Nonetheless, the introduction of CuL NCs led to a significant reduction in the increase in green fluorescence, suggesting that the decrease in MMP was prevented and apoptosis was inhibited. This was confirmed in both RAW264.7 and HT-29 cells (Fig. S16, Fig. S17, and Fig. S18).

Dysfunction of the intestinal epithelial barrier is an important feature in the onset and maintenance of IBD, but the dysregulation of oxidative stress and the inflammatory microenvironment hinder the repair of damaged mucosal wounds, which in turn exacerbates the disease [53]. Therefore, maintaining an intact epithelial barrier is crucial for preventing disease progression. We explored the growth capacity of damaged colonic epithelial cells under oxidative stress conditions, and as shown in Fig. S19A, NCM460 cells demonstrated low tendency to grow in H_2O_2 environment, whereas the recovery of NCM460 cells was significantly improved after treatment with 200 μg/mL of CuL NCs. CuL NCs exhibited a tendency to promote the growth of NCM460 cells compared to the control group (Fig. S19B); therefore, we also confirmed that CuL NCs could promote the expression of tight junction proteins Zonula Occludens protein 1 (ZO-1) and occludin in quantitative reverse transcription polymerase chain reaction (qRT-PCR) experiments (Figs. S19C and D). Moreover, lipid peroxidation damaged the membrane integrity of intestinal epithelial cells. The malondialdehyde (MDA) content is an important parameter that reflects the antioxidant capacity of organisms and indirectly reflects the degree of peroxidation injury in tissues and cells [54]. MDA levels in NCM460 cells were assessed. MDA production was markedly elevated in NCM460 cells after H_2O_2 treatment, suggesting the onset of severe oxidative stress. However, there was a decrease in MDA levels after the addition of CuL NCs (Fig. S19E). The abovementioned results demonstrate that CuL NCs are beneficial in counteracting the cellular damage caused by oxidative stress and protecting the intestinal epithelial cells while enhancing the epithelial barrier function by modifying the structure and functionality of tight junctions.

3.4. *Anti-inflammatory experiment In vitro*

Given the influence of oxidative stress in macrophage polarization on inflammation-related diseases and considering that previous studies have shown that proinflammatory M1 and anti-inflammatory M2 macrophages play a key role in the development of IBD [55]; *in vitro* studies were conducted to stimulate macrophage polarization with LPS to evaluate whether macrophage polarization during inflammatory periods can be modulated by CuL NCs. In Fig. 2H, compared with the LPS-stimulated group, the percentage of M2 cells after incubation with 100 and 200 μg/mL CuL NCs increased from 1.39 % to 11.1 % and 16.6 %, respectively. Mechanistically, Nrf2, an endogenous antioxidant pathway, is a spontaneously produced system against free radicals, and Nrf2 transcription factors have been reported to promote M2 polarization by activating potential signals through translocation from the cytoplasm to the nucleus. To explore this possibility, experiments revealed that the proportion of nuclear Nrf2 was notably elevated in macrophages treated with LPS after the administration of CuL NCs (Fig. 2I and Fig. S20). Although Nrf2 does not directly react with ROS, it can induce the expression of several antioxidant enzymes and protective proteins. The SOD content in RAW264.7 cells induced by LPS was tested using the SOD enzyme activity detection kit. The SOD activity in the LPS-induced inflammation model decreased by 20 ± 10.1 %. Conversely, the SOD level in the 200 μg/mL CuL NCs group returned to control group levels (Fig. 2J). Meanwhile, CuL NCs could also reverse the intracellular CAT activity levels after LPS treatment (Fig. 2K).

After confirming that CuL NCs promoted M2 polarization. The key inflammatory factors TNF-α, IL-1β, IL-6, and IL-17A were detected, with

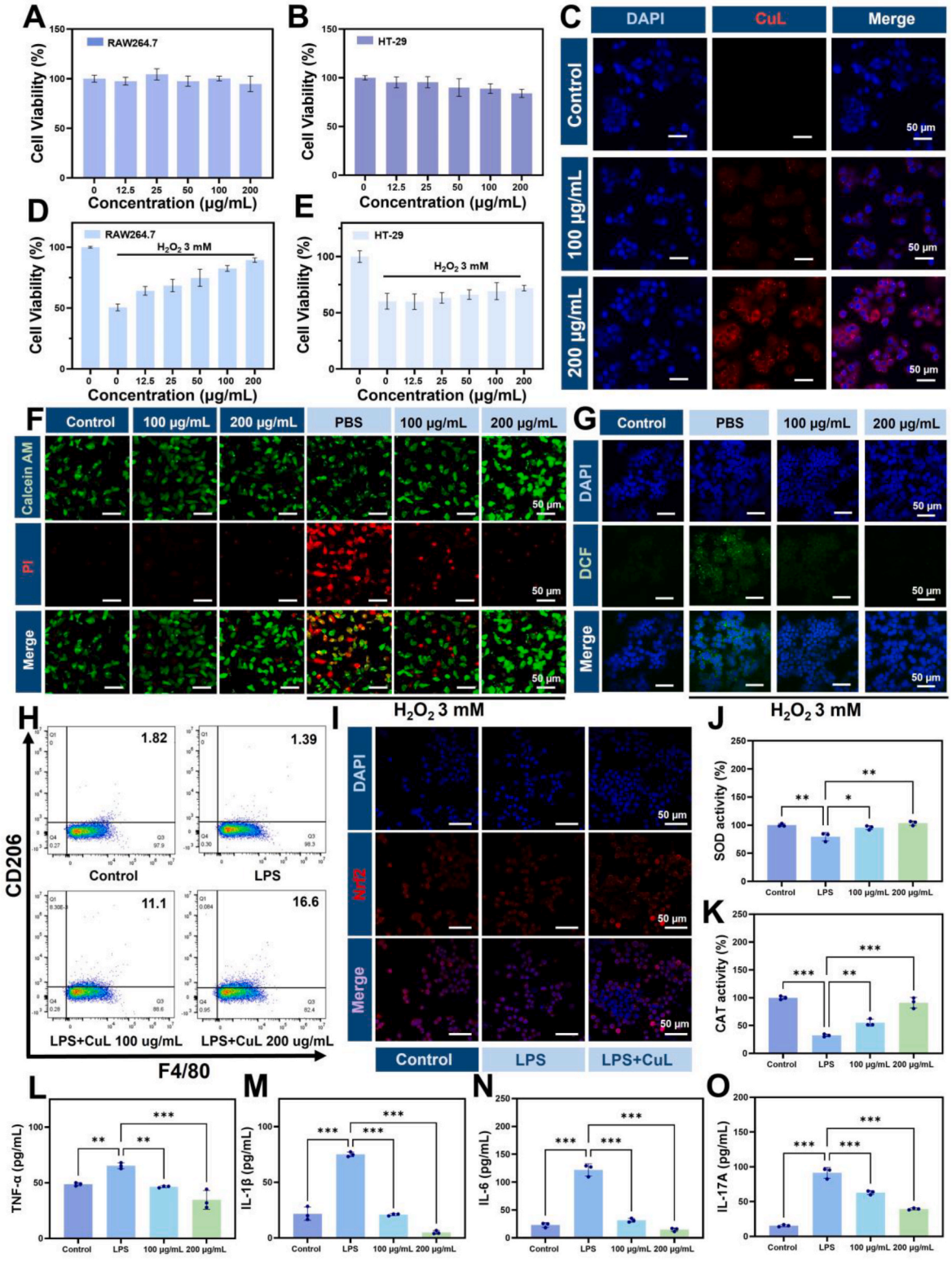

Fig. 2. Protective and anti-inflammatory effects of CuL NCs on cells *in vitro*. (A, B) Viability of RAW264.7 and HT-29 cells (n = 3). (C) CLSM images of RAW264.7 cell intracellular endocytosis; scale bars = 50 μm. (D, E) Viability of RAW264.7 and HT-29 cells followed by H_2O_2 incubation (n = 3). (F) Images of calcein AM/PI–stained RAW264.7 cells; scale bars = 50 μm. (G) CLSM images of ROS in RAW264.7 cells stained by DCFH-DA; scale bars = 50 μm. (H) The effect of CuL NCs on M2 was detected by flow cytometry. (I) Macrophages collected after different treatments for immunofluorescence staining of Nrf2 (CuL NCs: 200 μg/mL); scale bars = 50 μm. (J, K) SOD and CAT levels in RAW264.7 cells. Levels of (L) TNF-α, (M) IL-1β, (N) IL-6 and (O) IL-17A in RAW264.7 cells stimulated by LPS and treated with different concentrations of CuL NCs (n = 3).

levels reaching 65.3 ± 2.7, 74.9 ± 2.1, 121.9 ± 10.8, and 91.4 ± 7.8 pg/mL, respectively (Fig. 2L–**O**). CuL NCs significantly reduced the expression levels to 34.6 ± 8.5, 4.9 ± 1.5, 14.6 ± 3.1, and 39.5 ± 1.4 pg/mL, respectively. Beyond the effect of a reduced expression of proinflammatory cytokines, CuL NCs significantly increased the expression of the anti-inflammatory cytokines. The anti-inflammatory factors IL-10 and IL-4, which are markers of M2, were detected. In macrophages treated with LPS, IL-10 and IL-4 levels were relatively low at 7.5 ± 2.9 and 6.1 ± 4.4 pg/mL, respectively (Fig. S21). Conversely, these levels spiked significantly after treatment with CuL NCs. As anticipated, qRT-PCR results proved that CuL NCs could regulate the verification of the microenvironment (Fig. S22).

3.5. Biodistribution and biosafety In vivo

Before evaluating the prophylactic and protective effects of CuL NCs in acute enteritis, the biodistribution and metabolic pathways of CuL NCs were explored, as these are prerequisites for determining the dosage and frequency of administration. After intraperitoneal injection of Cy5.5-CuL NCs in healthy mice, *in vivo* imaging was evaluated using a small-animal imager at different time points. As shown in Fig. S23, fluorescence in the lower abdomen started to accumulate at around 2 h, reached a maximum intensity at the 12th hour, and then weakened after 24 h. Next, we explored the distribution of CuL NCs in specific organs by ICP-OES. The heart, liver, spleen, lungs, kidneys, and colon were collected at different time points for *in vitro* imaging studies. A large amount of CuL NCs reached the major organs through blood circulation, among which the accumulation in the liver and kidney was the highest. After 12 h, the content of CuL NCs in the major organs showed a downward trend, which may be related to the biodegradation of CuL NCs *in vivo*. After 48 h, CuL NCs were metabolized by the liver and kidneys and expelled from the body (Fig. S24).

To assess the biosafety of the formulation *in vivo*, we first performed a hemolysis test, which showed that all concentrations of CuL NCs dispersions had a hemolysis rate of <2 %, indicating excellent hemocompatibility (Fig. S25). Subsequently, *in vivo* toxicity was assessed through intraperitoneal injection of a 20 mg/kg of CuL NCs into healthy C57BL/6 mice every other day. After euthanizing the mice on day 7 and 14, major organs were collected for H&E staining. H&E results show that CuL NCs did not induce significant pathological changes or inflammatory lesions compared with those in control mice (Fig. S26). The hematological index parameters, such as mean corpuscular hematocrit (HCT), hemoglobin (HGB), mean corpuscular hemoglobin, red blood cells (RBCs), mean corpuscular hemoglobin concentration, white blood cells, and mean corpuscular volume, remained within the normal range for the CuL NCs–treated group and the control group, with no significant outliers (Fig. S27A). More importantly, typical hepatic and renal function parameters, namely, alanine aminotransferase (ALT), aspartate aminotransferase (AST), urea (UREA), uric acid, and total protein, did not exhibit significant abnormal values, suggesting that CuL NCs are virtually devoid of hepatotoxicity and nephrotoxicity (Fig. S27B).

3.6. Colitis Preventative effects of CuL NCs

Motivated by the powerful protective effect of CuL NCs on intestinal epithelial cells and good biological safety, the preventive potential of CuL NCs was investigated before the onset of colitis. Initially, healthy mice were allowed to acclimate. Subsequently, the mice were administered a 4 % DSS solution. At the same time, the mice were treated with different concentrations of CuL NCs, and the mice were sacrificed on day 9, with specific methods detailed in the experimental section (Fig. 3A). Mice treated with different concentrations of CuL NCs showed no significant differences in physiological parameters compared to the control group, indicating good biocompatibility of CuL NCs. Colon length, a key indicator of colitis progression, decreased to 6.0 ± 0.29 cm in the colitis group, but CuL NCs (5, 10, 20 mg/kg) restored the colon lengths to 7.9 ± 0.13, 8.7 ± 0.15, and 9.0 ± 0.13 cm, respectively (Fig. 3B and **C**). DSS-fed mice experienced marked weight loss, while the CuL NCs (20 mg/kg) group showed the least weight loss and a trend of increase in weight by day 7 (Fig. 3D). DAI was significantly increased in the DSS and low-dose CuL NCs groups, indicating severe diarrhea and blood in the stool (Fig. 3E). The high-dose CuL NCs group (20 mg/kg) showed a gradual increase in DAI, effectively suppressing IBD. H&E staining revealed inflammatory symptoms in DSS-induced mice, including mucosal erosion and cell damage (Fig. 3F). CuL NCs treatment restored colon length and alleviated microstructural damage, exhibiting protective effects on colonic tissue.

ROS were identified as a primary target for IBD treatment [11]. As shown in Fig. 3G, fluorescence staining with dihydroethidium (DHE) revealed no red fluorescence in the colons of healthy mice or those treated with CuL NCs, while colitis mice exhibited significant red fluorescence, indicating excessive ROS accumulation. In the CuL NCs treatment group, red fluorescence decreased with increasing drug concentration, demonstrating the efficacy of CuL NCs in reducing excess ROS in the colon and preventing colitis development. DSS-induced mice showed significantly reduced levels of CAT and SOD, suggesting a disrupted antioxidant system. CuL NCs treatment effectively restored these levels to 18.3 ± 0.5 and 15.1 ± 0.65 U/mL, respectively (Fig. 3H and **I**). MDA levels were elevated in DSS-treated mice but significantly decreased after CuL NCs treatment. Myeloperoxidase (MPO) activity, an indicator of neutrophil infiltration, was increased in the inflamed area (124.7 ± 9.32 ng/mL) but was restored to 58.9 ± 5.94 ng/mL after CuL NCs treatment (Figs. S28A and B). The levels of proinflammatory cytokines IL-1β, IL-6, TNF-α, and IL-17A were elevated in the DSS group compared to those on healthy mice but decreased in the CuL NCs–treated group (Fig. 3J–**M**). Conversely, the levels of anti-inflammatory cytokines IL-10 and IL-4 increased after CuL NCs treatment, enhancing the inflammatory microenvironment, suppressing local immune responses, and promoting colonic epithelial barrier restoration (Figs. S28C and D).

To further compare the therapeutic effects, we compared the results of 20-mg/kg CuL NCs–treated group with those of the Lut-treated group, PVP-treated group, Cu^{2+}-treated group as well as the clinically used IBD treatment drug 5-ASA (Fig. 3N). Results showed that the CuL NCs group most effectively inhibited colonic shortening in colitis mice and was the only treatment in these groups that directly reduced severe symptoms to mild symptoms in colitis mice (Fig. 3O and **P**). DSS induced IBD mice sustained weight loss within 8 days. Compared with other treatment groups, CuL NCs treated colitis mice showed significantly slower weight loss (Fig. 3Q). In addition, the reduction of DAI further illustrated the preventive efficacy of CuL NPs for IBD, with the same dose of 5-asa having a lower effect on DAI (Fig. 3R). Changes in tissue damage were direct evidence to evaluate the effectiveness of colitis treatment. The DSS group shown in Fig. 3T and **S** showed signs of lamina propria vasodilation, congestion, epithelial degeneration and necrosis, mucosal erosion, and diffuse mixed inflammatory cell infiltration of the mucous lamina propria. The CuL NCs treatment group showed better improvement compared to the other treatment groups. The above evidence showed that CuL NCs greatly improved the signs and symptoms of IBD, and the effect was significantly better than the positive control drug 5-ASA, Lut and Cu^{2+}.

3.7. Mechanism of CuL NCs treatment of colitis

Given the promising preventive effects of CuL NCs in the early stages of disease, we investigated their potential therapeutic effects after the disease onset by regulating biological pathways and promoting cellular repair. After 1 week of acclimatization, C57BL/6 mice were given a 4 % DSS solution. On day 9, 11, and 13, the mice received intraperitoneal injections of either PBS or CuL NCs (Fig. 4A). The colon length in the DSS-induced colitis group was significantly shorter than that in the

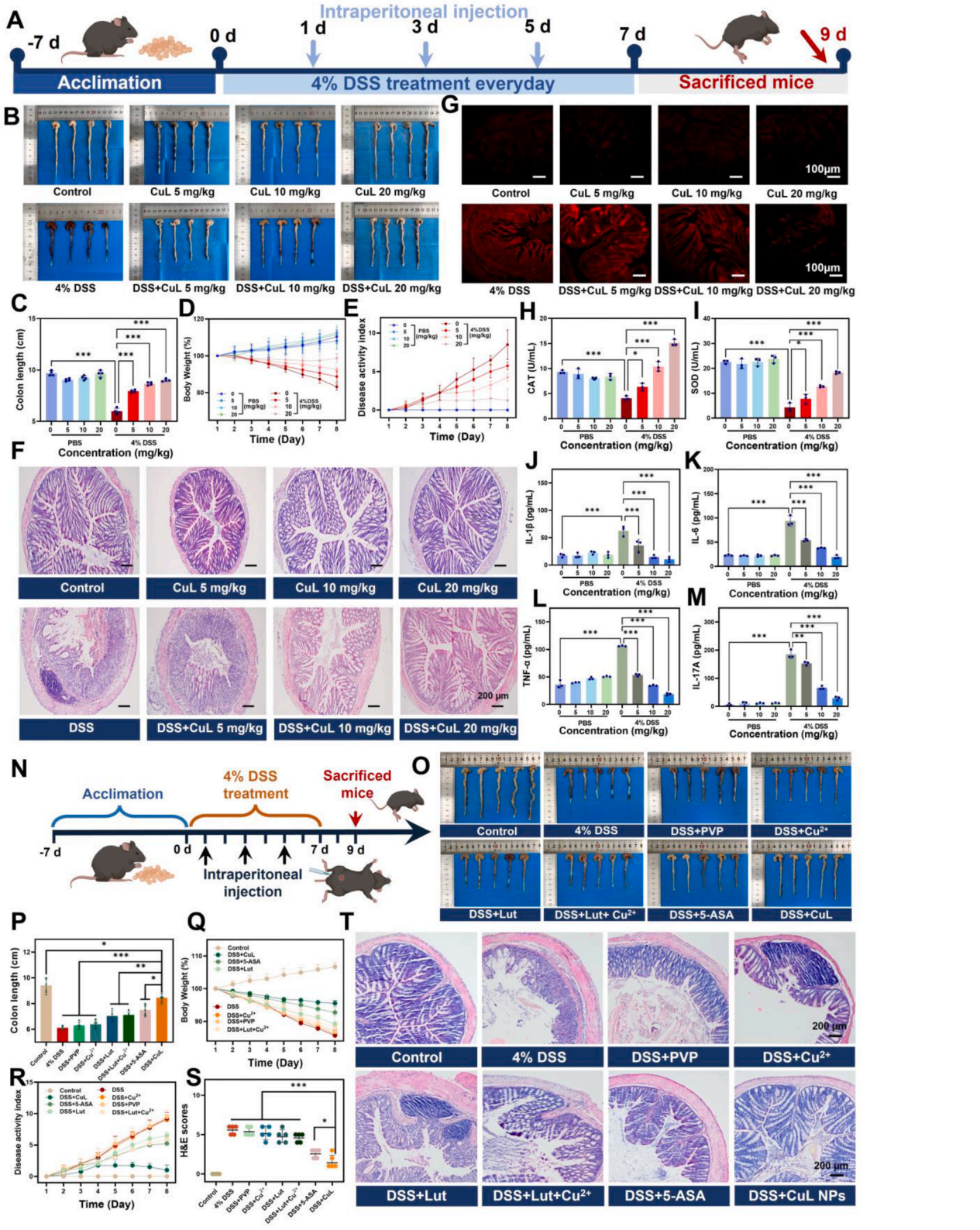

Fig. 3. Preventive effect of CuL NCs on IBD. (A) Experimental protocol. (B) Digital photos of the colons of each group of mice on day 9. (C) Colon length (n = 4). (D) Daily body weight (n = 4). (E) DAI scores in each group over 8 days (n = 4). (F) H&E staining images of the mouse colon; scale bars = 200 μm. (G) DHE fluorescence images of the colon in different groups of mice; scale bars = 100 μm. (H, I) SOD and CAT activity levels. (J–M) TNF-α, IL-1β, IL-6, and IL-17A levels in colon tissue. Data are shown as mean ± SD (n = 3). (N) Experimental protocol. (O) Digital photos of the colons of each group of mice on day 9. (P) Colon length (n = 5). (Q) Daily body weight (n = 5). (R) Daily body weight (n = 5). (S) H&E score (n = 5). (T) H&E staining of colon sections of mice in different treatment groups; scale bars = 200 μm.

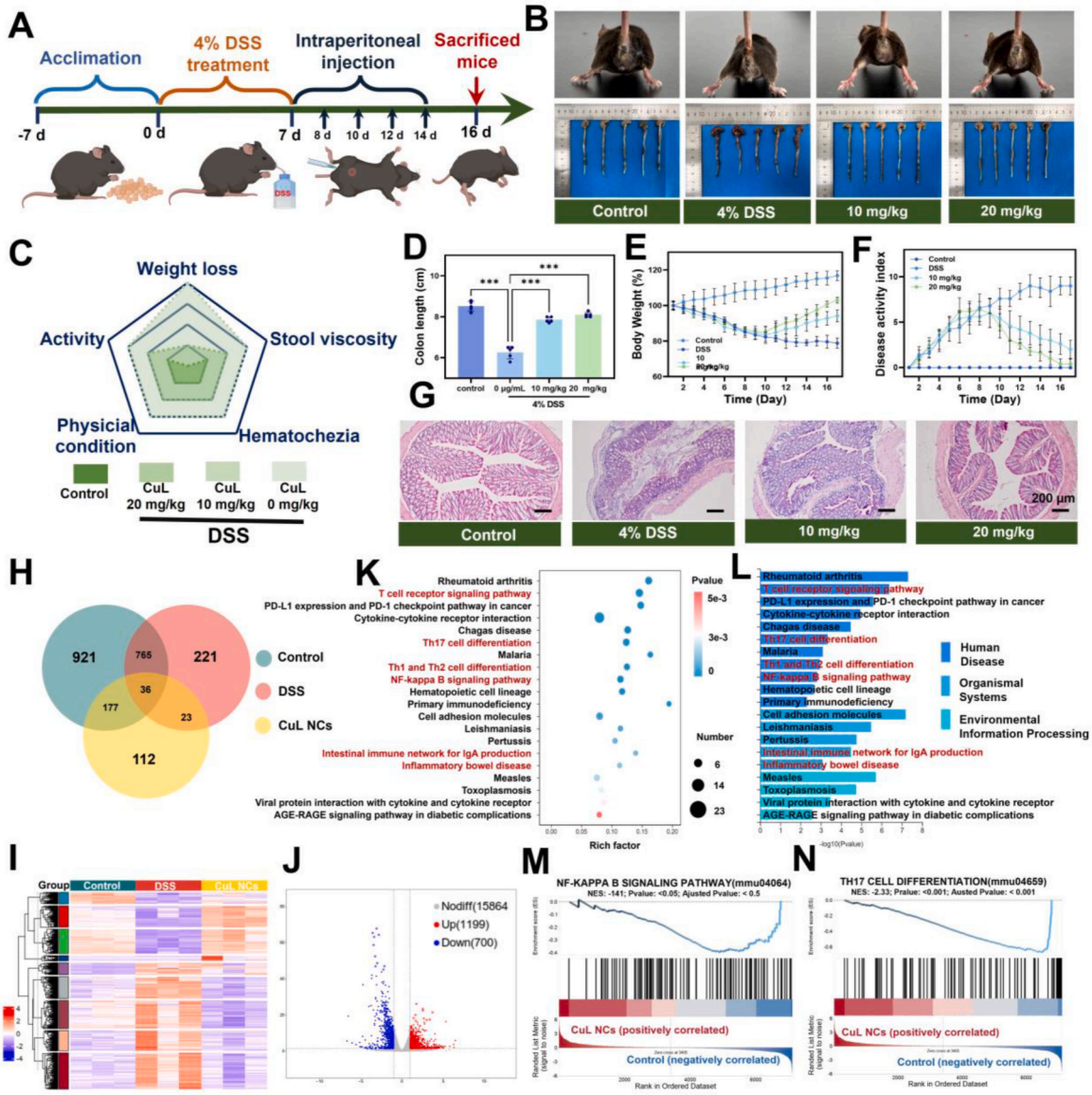

Fig. 4. CuL NCs treatment of mice with DSS-induced colitis. (A) Experimental protocol. (B) Digital photos of anus and colons of mice on day 16. (C) Status of mice scores. (D) Colon length (n = 5). (E) Daily body weight changes (n = 5). (F) DAI scores for each group over a period of 17 days (n = 5). (G) H&E images; scale bars = 200 μm. (H) Venn diagram of DEGs. (I) Heatmap analysis of DEGs. (J) Volcano plot of DEGs. (K, L) Kyoto Encyclopedia of Genes and Genomes (KEGG) enrichment of DEGs. (M, N) NF-κB and Th17 signaling pathway were selected for GSEA.

control group (Fig. 4B and **D**). Colitis mice showed signs of hemorrhagic diarrhea and weight loss, consistent with clinical symptoms (Fig. 4E). The DAI score significantly increased in the DSS group after 7 days but decreased in the CuL NCs group following treatment starting on day 9 (Fig. 4F). CuL NCs also significantly reduced colon shortening and weight loss, enhancing the quality of life of mice (Fig. 4C). H&E staining revealed pathological changes in the colonic tissue, including epithelial barrier defects, crypt damage, goblet cell depletion, and inflammatory cell infiltration, in the colitis group (Fig. G).

To better understand the therapeutic mechanism of CuL NCs against IBD, we conducted comprehensive RNA sequencing (RNA-seq) on colon tissues of healthy mice, CuL NCs-treated mice, and DSS-induced colitis mice. Venn diagrams illustrated the distinct transcriptome profiles of the control, DSS-induced colitis, and CuL NCs-treated groups (Fig. 4H). Differentially expressed genes (DEGs) showed clear clustering (Fig. 4I), with volcano plots indicating significant differences between the DSS-induced colitis and CuL NCs-treated groups, where 700 genes were downregulated and 1199 genes were upregulated (Fig. 4J). We performed KEGG enrichment analysis on the DEGs to identify the pathways through which CuL NCs exerted their immunomodulatory effects. The analysis revealed that the T-cell pathway, Th17 cell differentiation, Th1 and Th2 cell differentiation, and NF-κB signaling pathway were closely associated with the therapeutic mechanisms of CuL NCs (Fig. 4K and **L**). Additionally, genomic enrichment analysis (GSEA) showed that DEGs were clustered in pathways related to oxidative stress and inflammatory response compared to the DSS-induced colitis model. CuL NCs treatment reduced the expression of the inflammation-associated NF-κB pathway and inhibited Th17 cell differentiation (Fig. 4M and **N**).

Based on the findings regarding the role of NF-κB in oxidative stress and inflammation, as well as the effects of Lut on Nrf2, we hypothesized that CuL NCs may have inhibited inflammation by modulating the NF-κB/Nrf2 signaling pathway, thereby reducing the levels of proinflammatory factors and enhancing the expression of antioxidant genes (Fig. 5A). IHC was utilized to assess the expression levels and distribution of NF-κB in colon tissues. The increase in inhibitor of kappa B α

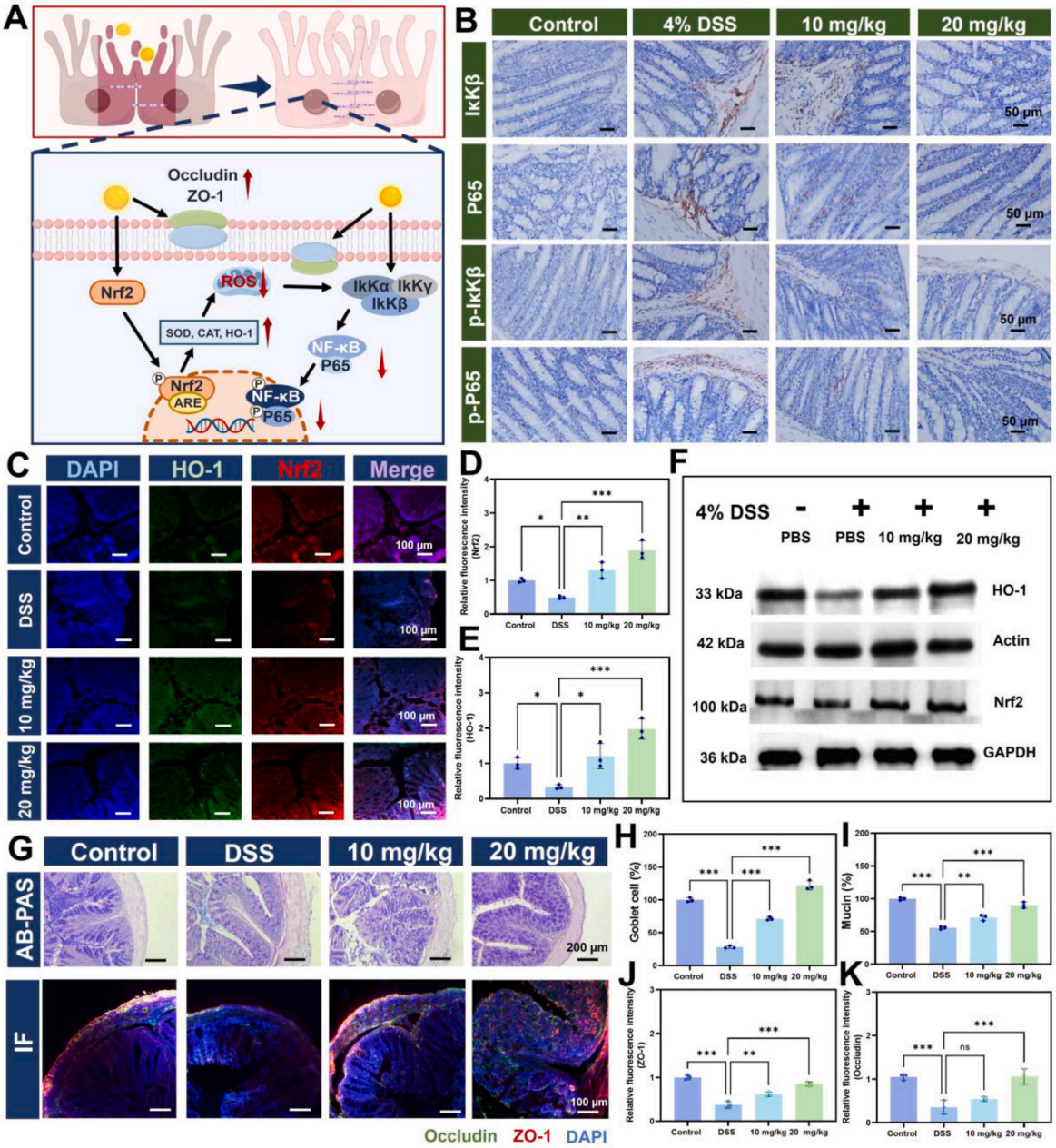

Fig. 5. Mechanism of CuL NCs treatment of colitis. (A) Therapeutic mechanism diagram of CuL NCs. (B) Immunohistochemical staining of IκKβ, p65, p-IκKβ, and p-p65; scale bars = 50 μm. (C) Immunofluorescence staining of HO-1 and Nrf2; scale bars = 100 μm. (D, E) Nrf2 and HO-1 quantification. (F) WB of HO-1 and Nrf2. (G) AB-PAS staining of the mouse colon; scale bars = 200 μm. Immunofluorescence images of ZO-1 and occludin; scale bars = 100 μm. (H, I) Levels of mucin and goblet cells in the colon. (J, K) ZO-1 and occludin quantification. Data are shown as mean ± SD (n = 3).

(IκBα) and p65 in the DSS-induced colitis model group was significantly attenuated by treatment groups (Fig. 5B). The levels of p-IκBα and p-p65, associated with the activation of the NF-κB signaling pathway, also returned to near normal levels following CuL NCs treatment. In previous cellular experiments, we verified that Nrf2 could be activated by CuL NCs. This primary regulator of oxidative stress activated the expression of the antioxidant enzyme HO-1 to further clear ROS, which plays a central role in triggering inflammation and activating the NF-κB signaling pathway in the inflammatory process [56–58]. To further confirm the CuL NCs effect on Nrf2 and its downstream signaling molecule HO-1 at the animal level, immunofluorescence staining was performed, showing that the fluorescence intensity of Nrf2/HO-1 was weaker after DSS-induced colitis (Fig. 5C–**E**). This indicated a lower expression level of Nrf2/HO-1. Conversely, the treatment group showed a stronger fluorescence signal, indicating that the effects of CuL NCs led to a slight upregulation of Nrf2/HO-1 expression in the inflammatory microenvironment, thereby activating the antioxidant system. Western blot (WB) analysis further confirmed that CuL NCs upregulated the expression of Nrf2/HO-1 (Fig. 5F). Some biomarkers of oxidative stress and inflammation also returned to normal (Fig. S29). Furthermore, the activation of Nrf2 may influence the activation of Th2 cells and the production of IL-4. Experimental evidence demonstrated that CuL NCs not only regulate IL-4 but also IL-10 (Fig. S30). Combined with the above results, CuL NCs had antioxidant and anti-inflammatory effects both *in vivo* and *in vitro*, promoting the expression of SOD, CAT, and HO-1 by up-regulating the Nrf2 antioxidant gene, and clearing intracellular reactive oxygen species, thus exhibiting antioxidant capacity. By promoting the nuclear translocation of Nrf2, the activation of the NF-κB

signaling pathway was inhibited, and the expression of IL-1β, TNF-α, and other pro-inflammatory factors was reduced. In addition, CuL NCs transformed macrophages from M1 type to M2 type and promoted the expression of anti-inflammatory factors.

Intestinal mucus serves as a protective barrier that maintains gut homeostasis. However, in patients with IBD, the secretion of intestinal mucus is impaired, leading to the thinning of the mucus layer, which renders the gut more susceptible to inflammation, bacteria, and other harmful substances [59]. The effect of CuL NCs on mucus secretion was investigated using AB-PAS staining. In Fig. 5G–a significant quantity of goblet cells were present in each crypt and mucins in healthy mice, and a continuous thick mucus layer covered the colon epithelium. Alternatively, a notable reduction in the quantity of goblet cells per crypt was noted, along with the disruption of the mucus layer in the IBD model mice. Administration of CuL NCs significantly ameliorated the massive depletion of goblet cells and mucins caused by DSS. The protective effect of the high dose of CuL NCs on the mucus barrier was more obvious (Fig. 5H and **I**). The expression levels of ZO-1 and occludin increased, indicating that the compromised intestinal barrier was restored (Fig. 5J and **K**).

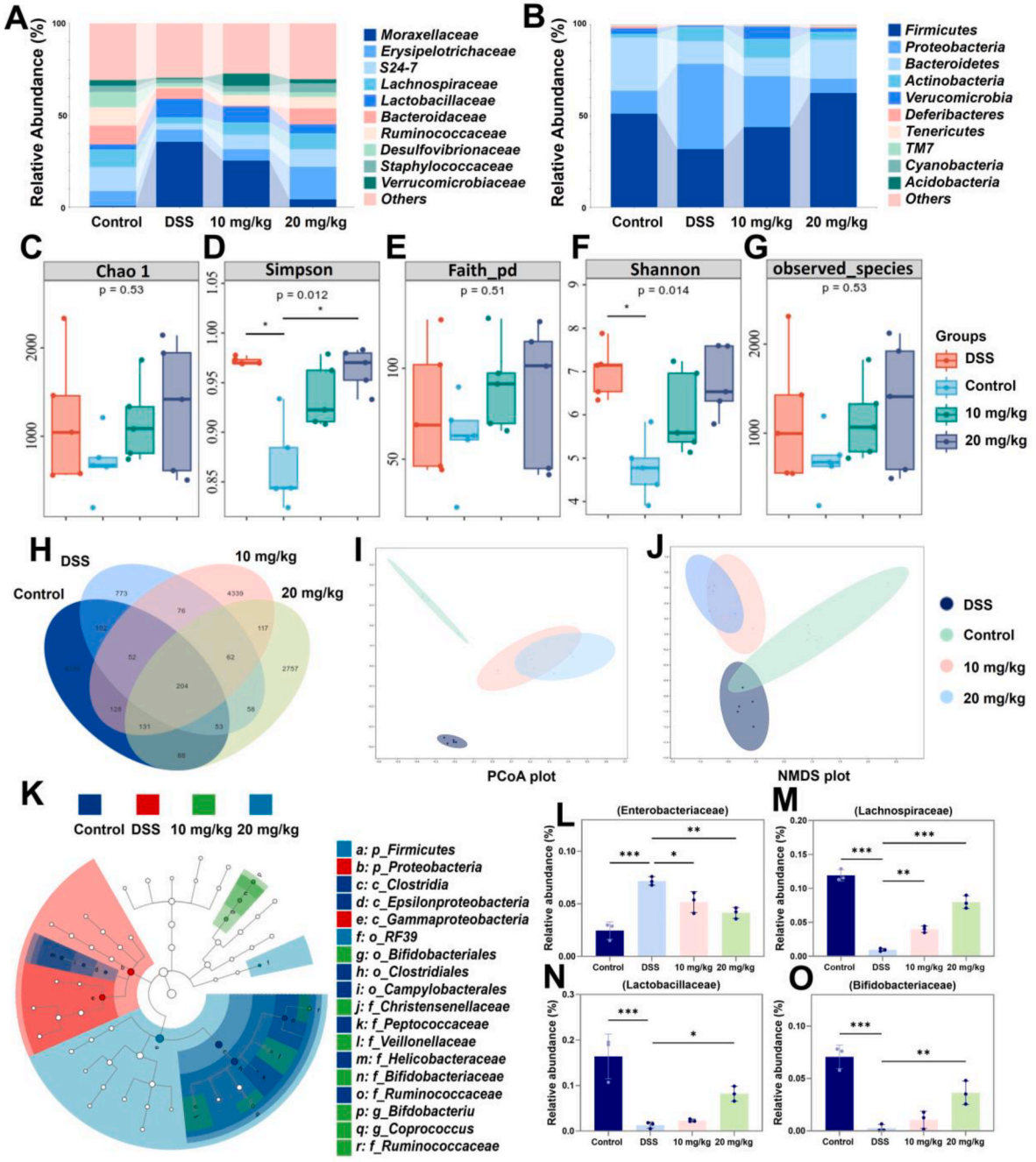

Fig. 6. Role of CuL NCs in regulating the intestinal flora. (A) Relative abundance of the top 20 gut microorganisms classified by family and (B) phylun level taxonomy. (C–G) α-Diversity of intestinal flora in mouse gut by Chao 1, Simpson, Faith-pd, Shannon and Observed-secies's index. (H) Venn diagram for the strains of identified bacteria in Control, DSS, and CuL NCs treated colitis mice. (I, J) β-diversity of faecal microbiome demonstrated by PCoA plot and NMDS plot. (K) Cladogram based on LEfSe analysis showing the communitycomposition of the gut microbiota in mice with different treatments. (L–O) The relative abundance of *Enterobacteriaceae* family, *Lachnospiraceae* family, *Lactobacillaceae* families and *Bifidobacteriaceae* family were selected in the family classification (n = 3).

3.8. Regulatory effect of CuL NCs on the intestinal flora

Increasing evidence indicates that the balance of gut microbiota not only influences the immune response of the intestine but also plays a crucial role in regulating inflammation, promoting digestion and nutrient absorption [60]. Therefore, maintaining gut homeostasis is essential for IBD treatment. The regulatory effects of CuL NCs on gut flora were investigated via 16S ribosomal RNA (16S rRNA) gene sequencing analysis to determine whether CuL NCs treatment could modulate the composition of intestinal flora in mice with IBD. In Fig. 6A and **B**, the microbiota composition of each group at the family and phylum levels is characterized by a significant decrease in harmful microorganisms such as Proteobacteria and a significant increase in beneficial bacteria such as *Bacteroides* [59]. These beneficial microbes support gut health by suppressing harmful microorganisms and regulating mucosal immune balance. In line with earlier studies,

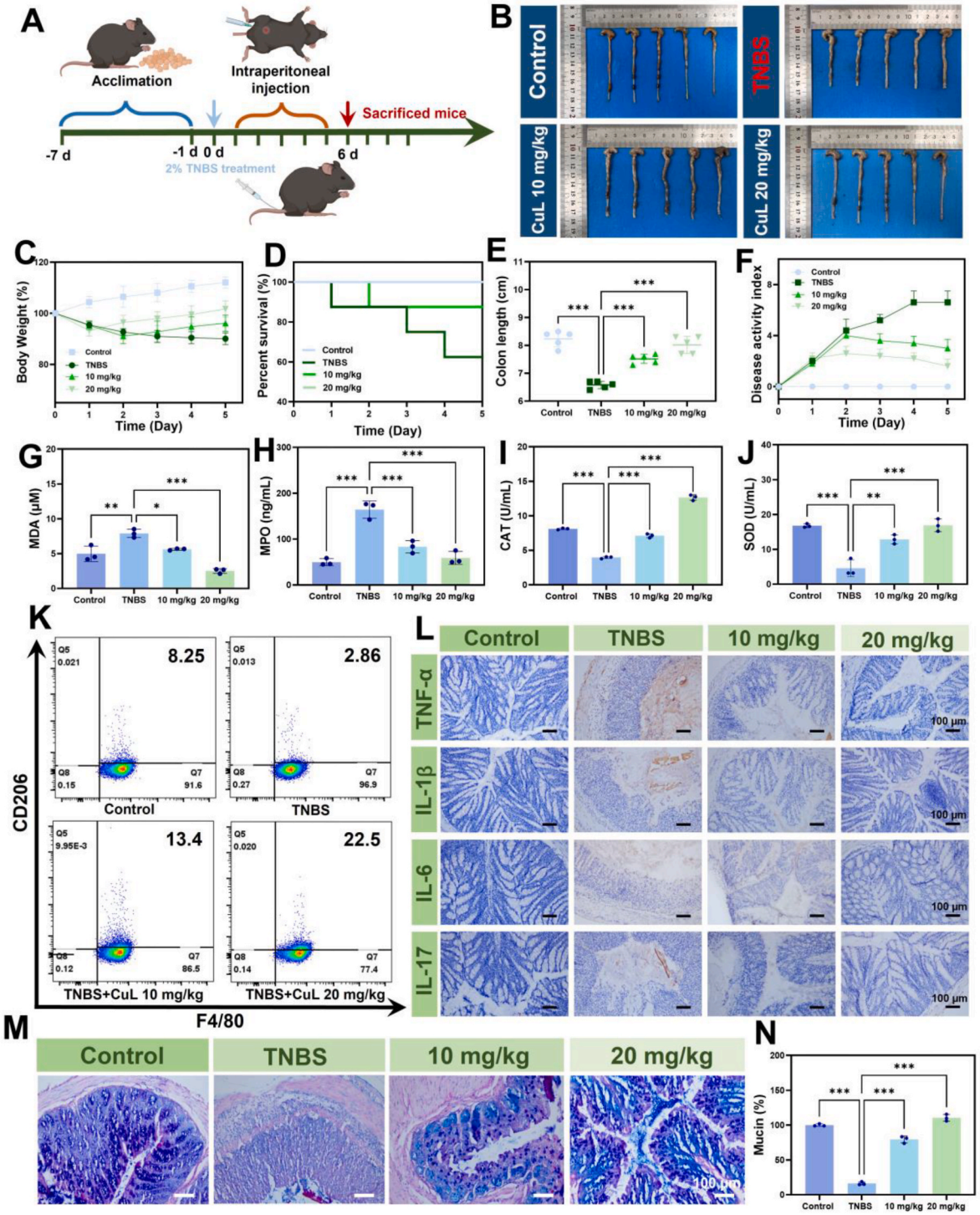

Fig. 7. CuL NCs treatment in TNBS-induced CD mice. (A) Overview of the experimental protocol. (B) Digital photos of the colons of each group of mice on day 6. (C) Body weight (n = 5). (D) Survival curve of mice (n = 8). (E) Colon length (n = 5). (F) DAI scores (n = 5). (G–J) MDA, MPO, CAT, and SOD levels in colon homogenates. (K) Flow cytometry analysis of macrophage inhibition in different subgroups after macrophage polarization. (L) Immunohistochemical staining of TNF-α, IL-1β, IL-6, and IL-17A; scale bars = 100 μm. (M) AB-PAS staining of colon; scale bars = 100 μm. (N) Mucin quantification (n = 3).

DSS-induced colitis was associated with a reduction in microbiota diversity and community richness, as evidenced by the α-diversity metrics (Chao 1, observed species, Shannon, Simpson, and Faith). However, treatment with CuL NCs resulted in a marked enhancement in both abundance and diversity of the gut microbiota of mice (Fig. 6C–**G**). This finding was also confirmed by bacterial abundance in terms of operational taxonomic units, and the bacterial abundance detected in both CuL NCs groups was much higher than that in the DSS-induced group (Fig. 6H). Subsequently, variations in microbiota composition among the samples were evaluated by β-diversity analysis. The principal coordinates analysis (PCoA) and nonmetric multidimensional scaling (NMDS) results showed that unique gut microbiota profiles were exhibited by the group receiving CuL NCs compared to the other treatment groups (Fig. 6I and **J**). Linear discriminant analysis (LDA) effect sizes were analyzed to identify taxa that were richly differentiated among these groups, and the LDA scores showed the dominant taxa and their effects at different taxonomic levels from phylum to genus (Fig. 6K).

In addition, the relative abundance of microbiota that changed at the family level was counted. Potentially harmful Proteobacteria, especially the *Enterobacteriaceae* family, was reduced by CuL NCs (Fig. 6L). The Enterobacteriaceae family consisted of bacteria that can thrive in an inflamed intestine, leading to over proliferation and further exacerbating the inflammatory response associated with IBD [59]. While the treatment with CuL NCs notably enhanced the relative abundance of Firmicutes, particularly within the *Lachnospiraceae* and *Lactobacillaceae* families (Fig. 6M and **N**). *Lachnospiraceae* is associated with butyric acid production, which promotes the growth of microorganisms and host epithelial cells [61,62]. *Bifidobacteriaceae* is a probiotic that benefits the health of the intestinal microenvironment by competitively inhibiting harmful microorganisms and modulating the intestinal immune response [63]. They have been found to be in higher abundance in the CuL NCs treatment group (Fig. 6O).

To sum up, CuL NCs are proposed as a potential prebiotic that promotes beneficial bacteria by altering the composition of the gut microbiota in mice and improving the intestinal ecological balance, thereby indirectly facilitating the amelioration of the intestinal inflammatory microenvironment. As a result, CuL NCs could serve as a promising option for treating active colitis by minimizing the side effects associated with antibiotics and helping prevent severe infections caused by drug-resistant bacteria.

3.9. CuL NCs for TNBS-induced CD

To explore the therapeutic uses of CuL NCs, their therapeutic efficacy against CD was further evaluated. As another type of IBD, CD was induced by rectal administration of TNBS in mice following typical procedures. Fig. 7A illustrated the overall experimental design of CuL NCs for the treatment of CD. First, the mice were fasted for 1 day before the establishment of CD. Then, the mice were treated with TNBS and ethanol enemas, and intraperitoneal injections of PBS or CuL NCs were performed daily for the next 5 days. The treatment effects were recorded and analyzed for all experimental groups. Differences in body weight changes, mortality, and colon length indicated the superior therapeutic effects of CuL NCs (Fig. 7C and **D**). Mice treated with CuL NCs lost less weight and exhibited decreased mortality compared to TNBS-induced mice, implying that CuL NCs significantly ameliorated the progression of TNBS-induced CD. The colon lengths of mice in the control, TNBS, TNBS +10-mg/kg CuL NCs, and TNBS +20-mg/kg CuL NCs groups were measured to be 8.2 ± 0.29, 6.6 ± 0.13, 7.5 ± 0.16, and 8.0 ± 0.30 cm, respectively. These findings suggest that CuL NCs significantly reduced colon length shortening in TNBS-treated mice (Fig. 7B and **E**). The scoring system further evaluated the therapeutic effects of CuL NCs (Fig. 7F). As illustrated in Fig. S31, CuL NCs provided significant protection against TNBS-induced colon damage in mice. This was supported by histological analyses. Specifically, the TNBS-treated mice exhibited severe mucosal damage, characterized by prominent infiltration of inflammatory cells and significant injury to the colonic epithelium. In stark contrast, treatment with CuL NCs effectively repaired the colonic epithelium and reconstructed the crypt structure. These results demonstrate the potential of CuL NCs in alleviating colonic damage. Furthermore, it was suspected that ROS clearance activity and effective therapeutic effects similar to those observed in DSS-induced colitis may be exhibited by CuL NCs in the context of TNBS-induced CD. In line with the expected results, the levels of SOD, CAT, MDA, and MPO detected in colon tissues of each group were decreased by CuL NCs treatment (Fig. 7G–**J**).

Subsequently, to demonstrate the effect of CuL NCs on macrophage polarization, the percentages of M1 and M2 cells in the colonic tissue were quantified. In Fig. S32, M1 cells during inflammation increased from 4.63 % in the normal group to 12.4 % in the TNBS group. After treatment with different concentrations of 10 mg/kg CuL NCs and 20 mg/kg CuL NCs, M1 cells decreased to 8.18 % and 3.54 %, respectively. Compared with TNBS-induced CD mice, the percentage of M2 cells increased from 2.86 % to 22.5 % after 20-mg/kg CuL NCs treatment (Fig. 7K). These findings indicate that CuL NCs can modify the balance between M1 and M2 macrophages, particularly promoting M2 polarization. Furthermore, we evaluated the levels of colonic proinflammatory cytokines through IHC to determine the impact of blocking the macrophage chemotaxis. Following TNBS-induced colitis, there was a significant increase in the production of IL-1β, IL-6, TNF-α, and IL-17A. However, CuL NCs treatment resulted in a reduction of these cytokines (Fig. 7I). Expression of transforming growth factor-β (TGF-β), which is activated in colitis-associated intestinal fibrosis, was also reduced after treatment (Figs. S33A and B) [64–66]. Treatment with CuL NCs promoted IL-4 and IL-10 production to a certain extent (Figs. S33C and D). The ELISA results similarly demonstrated modulation of anti-inflammatory and proinflammatory factors by CuL NCs treatment, all of which were restored from abnormal to normal levels after treatment (Fig. S34). In addition, intestinal barrier damage was inevitable during the pathogenesis of CD, and the repair of the intestinal barrier was significantly increased after CuL NCs treatment, which is manifested by the obvious increase in goblet cells and mucus secretion (Fig. 7M and **N**). These results demonstrated that CuL NCs potentially provide a novel approach to modulating the inflammatory processes associated with CD.

4. Conclusion

Herein, CuL NCs with good biosafety and biocompatibility have been successfully prepared through a simple hybrid approach, serving as ROS scavengers to modulate the intestinal inflammatory microenvironment. We have experimentally demonstrated that CuL NCs can effectively eliminate ROS, thereby protecting intestinal cells from damage. Furthermore, CuL NCs facilitate Nrf2 nuclear translocation, facilitating the transformation of macrophages into the anti-inflammatory M2 phenotype, thus increasing the anti-inflammatory factors in the inflammatory microenvironment. RNA-seq analysis reveals that CuL NCs suppress the NF-κB signaling pathway, clarifying the mechanism by which they protect the intestinal barrier from damage. Additionally, 16S rRNA analysis highlights their critical role in gut microbiota remodeling, demonstrating their ability to effectively reduce pathogenic bacteria while increasing beneficial probiotics. Therefore, CuL NCs can be considered a multifunctional and comprehensive nanomedicine that uniquely possesses the ability to simultaneously tackle oxidative stress, inflammation, mucosal barrier damage, and gut microbiota dysbiosis, representing a novel therapeutic approach for IBD. In summary, this work presents a novel nanoplatform composed of metal-natural product nanocomplexes that exhibit multifunctional properties and clinical translation potential. This innovative approach not only contributes to the development of new therapeutic strategies for IBD but also lays the groundwork for advanced antioxidant nanocomplexes applicable to a broader spectrum of inflammatory conditions.

CRediT authorship contribution statement

Wanyue Fu: Writing – original draft, Software, Resources, Methodology, Investigation, Formal analysis, Data curation, Conceptualization. **Zhongshi Huang:** Writing – original draft, Software, Methodology, Investigation, Formal analysis, Data curation. **Weiqi Li:** Methodology, Investigation, Formal analysis. **Lingling Xu:** Project administration, Methodology, Investigation, Formal analysis. **Miaomiao Yang:** Software, Investigation, Formal analysis. **Yan Ma:** Supervision, Software, Investigation, Formal analysis. **Hanghang Liu:** Supervision, Project administration, Investigation, Conceptualization. **Haisheng Qian:** Writing – review & editing, Supervision, Project administration. **Wanni Wang:** Supervision, Project administration, Funding acquisition, Formal analysis, Conceptualization.

Ethics approval and consent to participate

All animal experiments received approval from the Ethics Committee of Anhui Medical University (approval number: LLSC20241722).

Declaration of competing interest

The authors declare no conflict of interest.

Acknowledgements

This work was financially supported by the National Natural Science Foundation of China (Grants 82200610), the Natural Science Foundation of Hubei Province (2024AFB109) and the Basic and Clinical Cooperative Research and Promotion Program of Anhui Medical University (2021xkjT027).

Appendix A. Supplementary data

Supplementary data to this article can be found online at https://doi.org/10.1016/j.bioactmat.2024.12.004.

References

[1] G.G. Kaplan, J.W. Windsor, The four epidemiological stages in the global evolution of inflammatory bowel disease, Nat. Rev. Gastro. Hepat. 18 (2021) 56–66, https://doi.org/10.1038/s41575-020-00360-x.
[2] L. Xu, B.J. He, Y.X. Sun, J. Li, P. Shen, L.M. Hu, G.Z. Liu, J.X. Wang, L.P. Duan, S. Y. Zhan, S.F. Wang, Incidence of inflammatory bowel disease in urban China: a nationwide population-based study, Clin. Gastro. Hepat. 21 (2023) 13, https://doi.org/10.1016/j.cgh.2023.08.013.
[3] D.B. Graham, R.J. Xavier, Pathway paradigms revealed from the genetics of inflammatory bowel disease, Nature 578 (2020) 527–539, https://doi.org/10.1038/s41586-020-2025-2.
[4] R.S. Mehta, J.R. Mayers, Y.C. Zhang, A. Bhosle, N.R. Glasser, L.H. Nguyen, W. J. Ma, S. Bae, T. Branck, K.J. Song, L. Sebastian, J.A. Pacheco, H.S. Seo, C. Clish, S. Dhe-Paganon, A.N. Ananthakrishnan, E.A. Franzosa, E.P. Balskus, A.T. Chan, C. Huttenhower, Gut microbial metabolism of 5-ASA diminishes its clinical efficacy in inflammatory bowel disease, Nat. Med. 29 (2023) 700–709, https://doi.org/10.1038/s41591-023-02217-7.
[5] P. Eder, A. Zielinska, J. Karczewski, A. Dobrowolska, R. Slomski, E.B. Souto, How could nanobiotechnology improve treatment outcomes of anti-TNF-α therapy in inflammatory bowel disease? Current knowledge, future directions, J. Nanobiotechnol. 19 (2021) 346, https://doi.org/10.1186/s12951-021-01090-1.
[6] P.S. Haque, N. Kapur, T.A. Barrett, A.L. Theiss, Mitochondrial function and gastrointestinal diseases, Nat. Rev. Gastro. Hepat. 21 (2024) 537–555, https://doi.org/10.1038/s41575-024-00931-2.
[7] V. Marotti, Y.N. Xu, C.B. Michalowski, W.A. Zhang, I. Domingues, H. Ameraoui, T. G. Moreels, P. Baatsen, M. Van Hul, G.G. Muccioli, P.D. Cani, M. Alhouayek, A. Malfanti, A. Beloqui, A nanoparticle platform for combined mucosal healing and immunomodulation in inflammatory bowel disease treatment, Bioact. Mater. 32 (2024) 206–221, https://doi.org/10.1016/j.bioactmat.2023.09.014.
[8] T. Tian, Z.L. Wang, J.H. Zhang, Pathomechanisms of oxidative stress in inflammatory bowel disease and potential antioxidant therapies, Oxid. Med. Cell. Longev. 2017 (2017) 4535194, https://doi.org/10.1155/2017/4535194.
[9] J.R. Turner, Intestinal mucosal barrier function in health and disease, Nat. Rev. Immunol. 9 (2009) 799–809, https://doi.org/10.1038/nri2653.
[10] S. Citi, Intestinal barriers protect against disease, Science 359 (2018) 1097–1098, https://doi.org/10.1126/science.aat0835.
[11] H. Blaser, C. Dostert, T.W. Mak, D. Brenner, TNF and ROS crosstal in inflammation, Trends Cell Biol. 26 (2016) 249–261, https://doi.org/10.1016/j.tcb.2015.12.002.
[12] G. Rogler, Chronic ulcerative colitis and colorectal cancer, Cancer Lett. 345 (2014) 235–241, https://doi.org/10.1016/j.canlet.2013.07.032.
[13] J. Lloyd-Price, C. Arze, A.N. Ananthakrishnan, M. Schirmer, J. Avila-Pacheco, T. W. Poon, E. Andrews, N.J. Ajami, K.S. Bonham, C.J. Brislawn, D. Casero, H. Courtney, A. Gonzalez, T.G. Graeber, A.B. Hall, K. Lake, C.J. Landers, H. Mallick, D.R. Plichta, M. Prasad, G. Rahnavard, J. Sauk, D. Shungin, Y. Vázquez-Baeza, R.A. White, J. Braun, L.A. Denson, J.K. Jansson, R. Knight, S. Kugathasan, D. P.B. McGovern, J.F. Petrosino, T.S. Stappenbeck, H.S. Winter, C.B. Clish, E. A. Franzosa, H. Vlamakis, R.J. Xavier, C. Huttenhower, J. Bishai, K. Bullock, A. Deik, C. Dennis, J.L. Kaplan, H. Khalili, L.J. McIver, C.J. Moran, L. Nguyen, K. A. Pierce, R. Schwager, A. Sirota-Madi, B.W. Stevens, W. Tan, J.J. ten Hoeve, G. Weingart, R.G. Wilson, V. Yajnik, I. Investigators, Multi-omics of the gut microbial ecosystem in inflammatory bowel diseases, Nature 569 (2019) 655–662, https://doi.org/10.1038/s41586-019-1237-9.
[14] C. Le Berre, S. Honap, L. Peyrin-Biroulet, Ulcerative colitis, Lancet 402 (2023) 571–584, https://doi.org/10.1016/s0140-6736(23)00966-2.
[15] W.Y. Fu, L.L. Xu, Z.T. Chen, L.L. Kan, Y. Ma, H.S. Qian, W.N. Wang, Recent advances eon emerging nanomaterials for diagnosis and treatment of inflammatory bowel disease, J. Control. Release 363 (2023) 149–179, https://doi.org/10.1016/j.jconrel.2023.09.033.
[16] L. Li, P.L. Peng, N. Ding, W.H. Jia, C.H. Huang, Y. Tang, Oxidative stress, inflammation, gut dysbiosis: what can polyphenols do in inflammatory bowel disease? Antioxidants 12 (2023) 967, https://doi.org/10.3390/antiox12040967.
[17] Q.W. Chen, J.Y. Qiao, M.W. Cao, Z.Y. Han, X. Zeng, X.Z. Zhang, Spore germinator-loaded polysaccharide microspheres ameliorate colonic inflammation and tumorigenesis through remodeling gut microenvironment, Mater. Today 63 (2023) 32–49, https://doi.org/10.1016/j.mattod.2023.02.002.
[18] J.T. Li, J. Song, Z.C. Deng, J. Yang, X.Q. Wang, B.W. Gao, Y.Y. Zhu, M. Yang, D. P. Long, X.Q. Luo, M.X. Zhang, M.Z. Zhang, R.Q. Li, Robust reactive oxygen species modulator hitchhiking yeast microcapsules for colitis alleviation by trilogically intestinal microenvironment renovation, Bioact. Mater. 36 (2024) 203–220, https://doi.org/10.1016/j.bioactmat.2024.02.033.
[19] Z.H. Wu, S.M. Huang, T.T. Li, N. Li, D.D. Han, B. Zhang, Z.J.Z. Xu, S.Y. Zhang, J. M. Pang, S.L. Wang, G.L. Zhang, J.C. Zhao, J.J. Wang, Gut microbiota from green tea polyphenol-dosed mice improves intestinal epithelial homeostasis and ameliorates experimental colitis, Microbiome 9 (2021) 184, https://doi.org/10.1186/s40168-021-01115-9.
[20] M.H. Zu, D.C. Xie, B.S.B. Canup, N.X. Chen, Y.J. Wang, R.X. Sun, Z. Zhang, Y.M. Fu, F.Y. Dai, B. Xiao, 'Green' nanotherapeutics from tea leaves for orally targeted prevention and alleviation of colon diseases, Biomaterials 279 (2021) 121178, https://doi.org/10.1016/j.biomaterials.2021.121178.
[21] J.L. Fei, B. Liang, C.Z. Jiang, H.F. Ni, L.M. Wang, Luteolin inhibits IL-1β-induced inflammation in rat chondrocytes and attenuates osteoarthritis progression in a rat model, Biomed. Pharmacother. 109 (2019) 1586–1592, https://doi.org/10.1016/j.biopha.2018.09.161.
[22] H. Slika, H. Mansour, N. Wehbe, S.A. Nasser, R. Iratni, G. Nasrallah, A. Shaito, T. Ghaddar, F. Kobeissy, A.H. Eid, Therapeutic potential of flavonoids in cancer: ROS-mediated mechanisms, Biomed. Pharmacother. 146 (2022) 112442, https://doi.org/10.1016/j.biopha.2021.112442.
[23] L. Li, W. Luo, Y.Y. Qian, W.W. Zhu, J.C. Qian, J.L. Li, Y.Y. Jin, X.Z. Xu, G. Liang, Luteolin protects against diabetic cardiomyopathy by inhibiting NF-κB-mediated inflammation and activating the Nrf2-mediated antioxidant responses, Phytomedicine 59 (2019) 152774, https://doi.org/10.1016/j.phymed.2018.11.034.
[24] Y. Li, L. Shen, H.S. Luo, Luteolin ameliorates dextran sulfate sodium-induced colitis in mice possibly through activation of the Nrf2 signaling pathway, Int. Immunopharmacol. 40 (2016) 24–31, https://doi.org/10.1016/j.intimp.2016.08.020.
[25] A.R. Bourgonje, D. Kloska, A. Grochot-Przeczek, M. Feelisch, A. Cuadrado, H. van Goor, Personalized redox medicine in inflammatory bowel diseases: an emerging role for HIF-1α and NRF2 as therapeutic targets, Redox Biol. 60 (2023) 102603, https://doi.org/10.1016/j.redox.2023.102603.
[26] D. Ross, D. Siegel, The diverse functionality of NQO1 and its roles in redox control, Redox Biol. 41 (2021) 101950, https://doi.org/10.1016/j.redox.2021.101950.
[27] L. Torrente, G.M. DeNicola, Targeting NRF2 and its downstream processes: opportunities and challenges, Annu. Rev. Pharmacol. 62 (2022) 279–300, https://doi.org/10.1146/annurev-pharmtox-052220-104025.
[28] M.H. Zu, Y. Ma, B. Cannup, D.C. Xie, Y.J. Jung, J.M. Zhang, C.H. Yang, F. Gao, D. Merlin, B. Xiao, Oral delivery of natural active small molecules by polymeric nanoparticles for the treatment of inflammatory bowel diseases, Adv. Drug Deliver. Rev. 176 (2021) 113887, https://doi.org/10.1016/j.addr.2021.113887.
[29]a C. Tan, H. Fan, J.H. Ding, C.Q. Han, Y. Guan, F. Zhu, H. Wu, Y.J. Liu, W. Zhang, X. H. Hou, S.W. Tan, Q. Tang, ROS-responsive nanoparticles for oral delivery of luteolin and targeted therapy of ulcerative colitis by regulating pathological microenvironment, Mater, Today Bio 14 (2022) 100246, https://doi.org/10.1016/j.mtbio.2022.100246.
[29]b Z.Y. Chu, W.N. Wang, W. Zheng, W.Y. Fu, Y.J. Wang, H. Wang, H.S. Qian, Biomaterials with cancer cell-specific cytotoxicity: challenges and perspectives, Chem. Soc. Rev. 53 (2024) 8847–8877, https://doi.org/10.1039/d4cs00636d.
[30] C. Tan, H. Fan, J.H. Ding, C.Q. Han, Y. Guan, F. Zhu, H. Wu, Y.J. Liu, W. Zhang, X. H. Hou, S.W. Tan, Q. Tang, ROS-responsive nanoparticles for oral delivery of luteolin and targeted therapy of ulcerative colitis by regulating pathological microenvironment, Mater, Today Bio 14 (2022) 100246, https://doi.org/10.1016/j.mtbio.2022.100246.

[31] J.K. Gu, P.Y. Zhang, H.J. Li, Y.S. Wang, Y. Huang, L. Fan, X. Ma, X.D. Qian, J.Q. Xi, Cerium-luteolin nanocomplexes in managing inflammation-related diseases by antioxidant and immunoregulation, ACS Nano 18 (2024) 6229–6242, https://doi.org/10.1021/acsnano.3c09528.
[32] Y.X. Guo, Q. Sun, F.G. Wu, Y.L. Dai, X.Y. Chen, Polyphenol-containing nanoparticles: synthesis, properties, and therapeutic delivery, Adv. Mater. 33 (2021) 2007356, https://doi.org/10.1002/adma.202007356.
[33] Z.Y. Han, Q.W. Chen, D.W. Zheng, K.W. Chen, Q.X. Huang, Z.N. Zhuang, X. Z. Zhang, Inhalable capsular polysaccharide-camouflaged gallium-polyphenol nanoparticles enhance lung cancer chemotherapy by depleting local lung microbiota, Adv. Mater. 35 (2023) 2302551, https://doi.org/10.1002/adma.202302551.
[34] T.F. Liu, B.W. Xiao, F. Xiang, J.L. Tan, Z. Chen, X.R. Zhang, C.Z. Wu, Z.W. Mao, G. X. Luo, X.Y. Chen, J. Deng, Ultrasmall copper-based nanoparticles for reactive oxygen species scavenging and alleviation of inflammation related diseases, Nat. Commun. 11 (2020) 2788, https://doi.org/10.1038/s41467-020-16544-7.
[35] Z.Z. Zhang, Y. Pan, Z.Y. Guo, X. Fan, Q.Q. Pan, W.X. Gao, K. Luo, Y.J. Pu, B. He, An olsalazine nanoneedle-embedded inulin hydrogel reshapes intestinal homeostasis in inflammatory bowel disease, Bioact. Mater. 33 (2024) 71–84, https://doi.org/10.1016/j.bioactmat.2023.10.028.
[36] R. Thibault, P. De Coppet, K. Daly, A. Bourreille, M. Cuff, C. Bonnet, J.F. Mosnier, J.P. Galmiche, S. Shirazi-Beechey, J.P. Segain, Down-regulation of the monocarboxylate transporter 1 is involved in butyrate deficiency during intestinal inflammation, Gastroenterology 133 (2007) 1916–1927, https://doi.org/10.1053/j.gastro.2007.08.041.
[37] Q. Huang, Y.Q. Yang, Y. Zhu, Q.H. Chen, T.J. Zhao, Z.X. Xiao, M.Y. Wang, X. P. Song, Y.T. Jiang, Y.R. Yang, J.P. Zhang, Y. Xiao, Y.Y. Nan, W. Wu, K.L. Ai, Oral metal-free melanin nanozymes for natural and durable targeted treatment of inflammatory bowel disease (IBD), Small 19 (2023) 2207350, https://doi.org/10.1002/smll.202207350.
[38] S. Zhao, Y.X. Li, Q.Y. Liu, S.R. Li, Y. Cheng, C.Q. Cheng, Z.Y. Sun, Y. Du, C.J. Butch, H. Wei, An orally administered CeO_2@Montmorillonite nanozyme targets inflammation for inflammatory bowel disease therapy, Adv. Funct. Mater. 30 (2020) 2004692, https://doi.org/10.1002/adfm.202004692.
[39] A.H.C. Bai, W.K.K. Wu, L.L. Xu, S.H. Wong, M.Y. Go, A.W.H. Chan, M. Harbord, S. H. Zhang, M.H. Chen, J.C.Y. Wu, M.W.Y. Chan, M.T.V. Chan, F.K.L. Chan, J.J. Y. Sung, J. Yu, A.S.L. Cheng, S.C. Ng, Dysregulated lysine acetyltransferase 2B promotes inflammatory bowel disease pathogenesis through transcriptional repression of interleukin-10, J. Crohns Colitis 10 (2016) 726–734, https://doi.org/10.1093/ecco-jcc/jjw020.
[40] L. Malacaria, C. La Torre, E. Furia, A. Fazio, M.C. Caroleo, E. Cione, L. Gallelli, T. Marino, P. Plastina, Aluminum(III), iron(III) and copper(II) complexes of luteolin: stability, antioxidant, and anti-inflammatory properties, J. Mol. Liq. 345 (2022) 117895, https://doi.org/10.1016/j.molliq.2021.117895.
[41] H. Zhang, G.H. Li, Z.P. Su, Y.J. Bao, J.C. Wang, R. Yan, C.H. Guo, Y.X. Jin, Copper-doped luteolin carbon dots with antitumor properties based on the induction of immunogenic cell death, ACS Appl. Nano Mater. 7 (2024) 7942–7957, https://doi.org/10.1021/acsanm.4c00546.
[42] W.W. Feng, X.Y. Guo, G. Yang, Y. Yao, L.X. Zhao, S. Gao, F. Ye, Y. Fu, Direct electrospinning for producing multiple activity nanofibers consisting of aggregated luteolin/hydroxypropyl-gamma-cyclodextrin inclusion complex, Int. J. Biol. Macromol. 270 (2024) 132344, https://doi.org/10.1016/j.ijbiomac.2024.132344.
[43] R. Bulánek, R. Hrdina, A.F. Hassan, Preparation of polyvinylpyrrolidone modified nanomagnetite for degradation of nicotine by heterogeneous Fenton process, J. Environ. Chem. Eng. 7 (2019) 102988, https://doi.org/10.1016/j.jece.2019.102988.
[44] C.M. Yang, K. Chathuranga, J.S. Lee, W.H. Park, Effects of polyphenols on the thermal decomposition, antioxidative, and antimicrobial properties of poly(vinyl alcohol) and poly(vinyl pyrrolidone), Polym. Test. 116 (2022) 107786, https://doi.org/10.1016/j.polymertesting.2022.107786.
[45] H. Dong, X.C. Yang, J.P. He, S. Cai, K.J. Xiao, L. Zhu, Enhanced antioxidant activity, antibacterial activity and hypoglycemic effect of luteolin by complexation with manganese(II) and its inhibition kinetics on xanthine oxidase, RSC Adv. 7 (2017) 53385–53395, https://doi.org/10.1039/c7ra11036g.
[46] H. Huang, S.Q. Xie, L. Deng, J. Yuan, R.R. Yue, J.K. Xu, Fabrication of rGO/MXene-Pd/rGO hierarchical framework as high-performance electrochemical sensing platform for luteolin detection, Microchim. Acta 189 (2022) 59, https://doi.org/10.1007/s00604-021-05132-1.
[47] B. Dinesh, R. Saraswathi, Electrochemical synthesis of nanostructured copper-curcumin complex and its electrocatalytic application towards reduction of 4-nitrophenol, Sens. Actuator B-Chem. 253 (2017) 502–512, https://doi.org/10.1016/j.snb.2017.06.149.
[48] Y. Xu, J. Yang, Y. Lu, L.L. Qian, Z.Y. Yang, R.M. Han, J.P. Zhang, L.H. Skibsted, Copper(II) coordination and translocation in luteolin and effect on radical scavenging, J. Phys. Chem. B 124 (2020) 380–388, https://doi.org/10.1021/acs.jpcb.9b10531.
[49] M.Y. Wen, T.Y. Wang, N. Li, Y.F. Wu, L.B. Zhang, Y.M. Xue, L. Shang, Polyphenol-copper derived self-cascade nanozyme hydrogel in boosting oxygenation and robust revascularization for tissue regeneration, Adv. Funct. Mater. 34 (2024) 2403634, https://doi.org/10.1002/adfm.202403634.
[50] X.J. Cao, S. Tao, W.T. Wang, S.L. Wu, Y. Hong, X.Y. Wang, Y. Ma, H.S. Qian, Z. B. Zha, Ternary inulin hydrogel with long-term intestinal retention for simultaneously reversing IBD and its fibrotic complication, Nat. Commun. 15 (2024) 8428, https://doi.org/10.1038/s41467-024-52722-7.
[51] D.D. Zhu, H.T. Wu, K. Jiang, Y.F. Xu, Z.H. Miao, H. Wang, Y. Ma, Zero-valence selenium-enriched prussian blue nanozymes reconstruct intestinal barrier against inflammatory bowel disease via inhibiting ferroptosis and T cells differentiation, Adv. Healthc. Mater. 12 (2023) 2203160, https://doi.org/10.1002/adhm.202203160.
[52] H. Lee, J.H. Jeon, E.S. Kim, Mitochondrial dysfunctions in T cells: focus on inflammatory bowel disease, Front. Immunol. 14 (2023) 1219422, https://doi.org/10.3389/fimmu.2023.1219422.
[53] A. Larabi, N. Barnich, H.T.T. Nguyen, New insights into the interplay between autophagy, gut microbiota and inflammatory responses in IBD, Autophagy 16 (2020) 38–51, https://doi.org/10.1080/15548627.2019.1635384.
[54] M.X. Zhou, W.M. Xu, J.Z. Wang, J.K. Yan, Y.Y. Shi, C. Zhang, W.S. Ge, J. Wu, P. Du, Y.W. Chen, Boosting mTOR-dependent autophagy via upstream TLR4-MyD88-MAPK signalling and downstream NF-κB pathway quenches intestinal inflammation and oxidative stress injury, EBioMedicine 35 (2018) 345–360, https://doi.org/10.1016/j.ebiom.2018.08.035.
[55] M. Arabpour, A. Saghazadeh, N. Rezaei, Anti-inflammatory and M2 macrophage polarization-promoting effect of mesenchymal stem cell-derived exosomes, Int. Immunopharmacol. 97 (2021) 107823, https://doi.org/10.1016/j.intimp.2021.107823.
[56] A. Loboda, M. Damulewicz, E. Pyza, A. Jozkowicz, J. Dulak, Role of Nrf2/HO-1 system in development, oxidative stress response and diseases: an evolutionarily conserved mechanism, Cell. Mol. Life Sci. 73 (2016) 3221–3247, https://doi.org/10.1007/s00018-016-2223-0.
[57] L.P. Bao, J.S. Li, D.Q. Zha, L. Zhang, P. Gao, T. Yao, X.Y. Wu, Chlorogenic acid prevents diabetic nephropathy by inhibiting oxidative stress and inflammation through modulation of the Nrf2/HO-1 and NF-κB pathways, Int. Immunopharmacol. 54 (2018) 245–253, https://doi.org/10.1016/j.intimp.2017.11.021.
[58] Z.P. Shi, X.H. Li, J.F. Chen, Z.D. Dai, Y.F. Zhu, T. Wu, Q. Liu, H.L. Qin, Y. Zhang, H. R. Chen, Enzyme-like biomimetic oral-agent enabling modulating gut microbiota and restoring redox homeostasis to treat inflammatory bowel disease, Bioact. Mater. 35 (2024) 167–180, https://doi.org/10.1016/j.bioactmat.2024.01.016.
[59] J.K. Gustafsson, M.E.V. Johansson, The role of goblet cells and mucus in intestinal homeostasis, Nat. Rev. Gastroenterol. Hepatol. 19 (2022) 785–803, https://doi.org/10.1038/s41575-022-00675-x.
[60] D.W. Zheng, J.Y. Qiao, J.C. Ma, J.X. An, C.H. Yang, Y. Zhang, Q. Cheng, Z.Y. Rao, S.M. Zeng, L. Wang, X.Z. Zhang, A microbial community cultured in gradient hydrogel for investigating gut microbiome-drug interaction and guiding therapeutic decisions, Adv. Mater. 35 (2023) 2300977, https://doi.org/10.1002/adma.202300977.
[61] P. Gonçalves, J.R. Araújo, J.P. Di Santo, A cross-talk between microbiota-derived short-chain fatty acids and the host mucosal immune system regulates intestinal homeostasis and inflammatory bowel disease, Inflamm. Bowel Dis. 24 (2018) 558–572, https://doi.org/10.1093/ibd/izx029.
[62] D.W. Zheng, R.Q. Li, J.X. An, T.Q. Xie, Z.Y. Han, R. Xu, Y. Fang, X.Z. Zhang, Prebiotics-encapsulated probiotic spores regulate gut microbiota and suppress colon cancer, Adv. Mater. 32 (2020) 2004529, https://doi.org/10.1002/adma.202004529.
[63] A.S. Neish, Microbes in gastrointestinal health and disease, Gastroenterology 136 (2009) 65–80, https://doi.org/10.1053/j.gastro.2008.10.080.
[64] Y. Wang, Z. Wang, H.P. Yang, S.Z. Chen, D.K. Zheng, X.Y. Liu, Q.R. Jiang, Y. Chen, Metformin ameliorates chronic colitis-related intestinal fibrosis *via* inhibiting TGF-β1/smad3 signaling, Front. Pharmacol. 13 (2022) 887497, https://doi.org/10.3389/fphar.2022.887497.
[65] J.Y. Liu, Y.N. Bai, Y.G. Li, X.L. Li, K. Luo, Reprogramming the immunosuppressive tumor microenvironment through nanomedicine: an immunometabolism perspective, EBioMedicine 107 (2024) 105301, https://doi.org/10.1016/j.ebiom.2024.105301.
[66] H.N. Li, Q.Y. Gong, K. Luo, Biomarker-driven molecular imaging probes in radiotherapy, Theranostics 14 (2024) 4127–4146, https://doi.org/10.7150/thno.97768.